iScience

CellPress
OPEN ACCESS

Article

CDK7 Mediates the Beta-Adrenergic Signaling in Thermogenic Brown and White Adipose Tissues

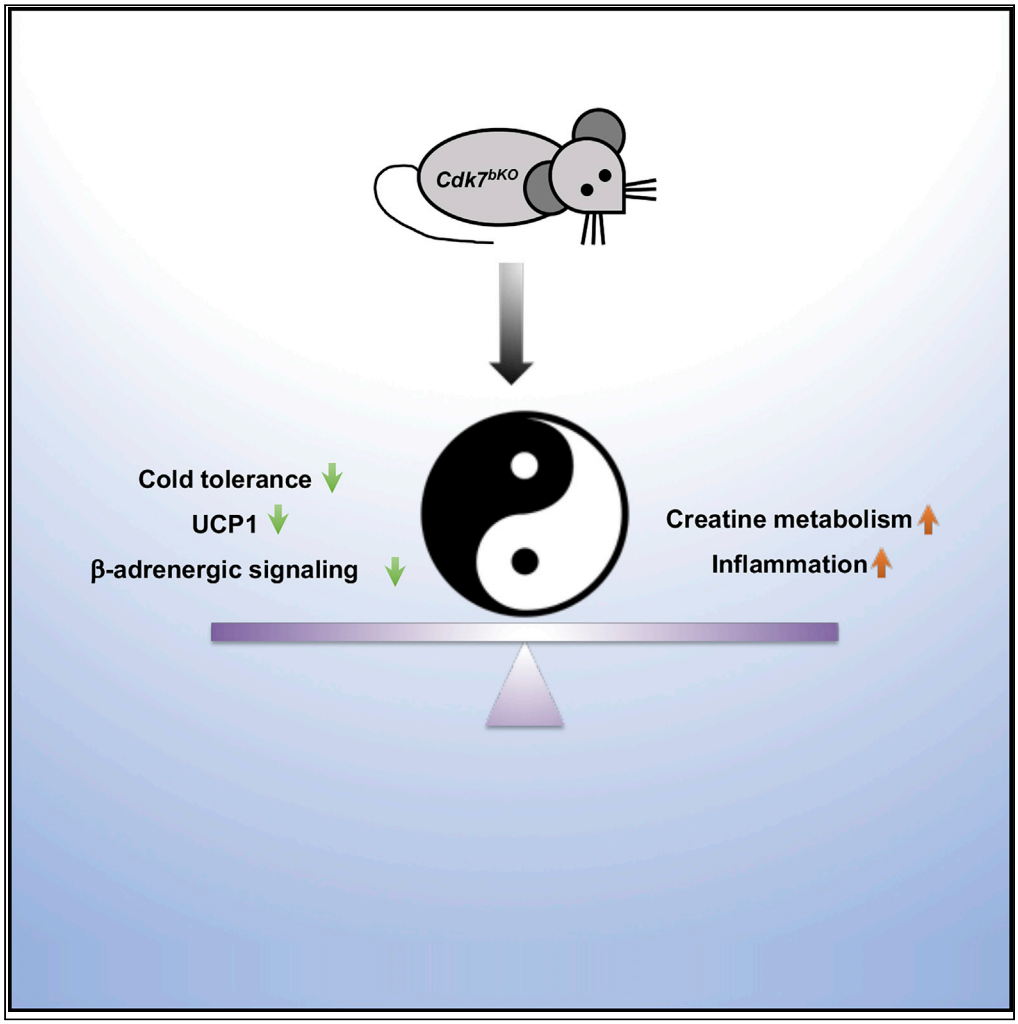

Honglei Ji, Yizhe Chen, Judit Castillo-Armengol, ..., Isabel C. Lopez-Mejia, Pierre-Damien Denechaud, Lluis Fajas

lluis.fajas@unil.ch

HIGHLIGHTS

CDK7 brown fat-specific knockout mice are cold intolerant

CDK7 is required for β-adrenergic signaling activation in response to cold

Creatine metabolism compensates for the impairment of thermogenesis in *Cdk7*^{bKO} mice

CDK7 mediates in the response to β3-adrenoceptor agonist in white adipose tissue

Ji et al., iScience *23*, 101163
June 26, 2020
https://doi.org/10.1016/j.isci.2020.101163

iScience

CellPress
OPEN ACCESS

Article

CDK7 Mediates the Beta-Adrenergic Signaling in Thermogenic Brown and White Adipose Tissues

Honglei Ji,[1,5] Yizhe Chen,[1,2,5] Judit Castillo-Armengol,[1] René Dreos,[1] Catherine Moret,[1] Guy Niederhäuser,[1] Brigitte Delacuisine,[1] Isabel C. Lopez-Mejia,[1] Pierre-Damien Denechaud,[1,3] and Lluis Fajas[1,4,6,*]

SUMMARY

Cyclin-dependent kinases (CDKs) are emerging regulators of adipose tissue metabolism. Here we aimed to explore the role of CDK7 in thermogenic fat. We found that CDK7 brown adipose tissue (BAT)-specific knockout mice (*Cdk7*^{bKO}) have decreased BAT mass and impaired β3-adrenergic signaling and develop hypothermia upon cold exposure. We found that loss of CDK7 in BAT disrupts the induction of thermogenic genes in response to cold. However, *Cdk7*^{bKO} mice do not show systemic metabolic dysfunction. Increased expression of genes of the creatine metabolism compensates for the heat generation in the BAT of *Cdk7*^{bKO} mice in response to cold. Finally, we show that CDK7 is required for beta 3-adrenergic agonist-induced browning of white adipose tissue (WAT). Indeed, *Cdk7* ablation in all adipose tissues (*Cdk7*^{aKO}) has impaired browning in WAT. Together, our results demonstrate that CDK7 is an important mediator of beta-adrenergic signaling in thermogenic brown and beige fat.

INTRODUCTION

Brown adipose tissue (BAT) is the main organ for non-shivering thermogenesis, which helps homeothermic vertebrates to maintain constant body temperature in changing nutritional and environmental conditions. Cold exposure leads the release by the sympathetic nervous system of norepinephrine in BAT, which binds to the β-adrenergic receptors, activates downstream signaling pathways, and ultimately leads to the induction of the thermogenic program (Cannon and Nedergaard, 2004). In addition, beige adipocytes, which also participate in non-shivering thermogenesis, emerge within white adipose tissue upon different stimuli, such as chronic cold acclimation or long-term β-adrenergic stimulation (Kajimura et al., 2015). Brown and beige fat activation rely on the action of uncoupling protein 1 (UCP1), which dissipates energy as heat instead of ATP production (Fedorenko et al., 2012). Recently, other UCP-independent alternative thermogenesis mechanisms have been described in brown and beige adipocytes, notably the creatine kinase-mediated futile cycling (Kazak et al., 2015, 2017, 2019), the triglyceride-fatty acid cycling (Granneman et al., 2003), and the SERCA2b-mediated calcium cycling (Ikeda et al., 2017).

Cyclin-dependent kinases (CDKs) are key regulators of the cell cycle progression. During G1 progression, pro-mitotic signals such as growth factors induce synthesis of D-type cyclins (cyclin D1, D2, and D3), which bind and activate CDK4/6 to trigger the phosphorylation of the retinoblastoma protein family, which includes pRB and other pocket proteins (i.e., p107 and p130). RB phosphorylation releases the E2F transcription factors, which promote the transcription of genes required for subsequent cell cycle progression (Malumbres and Barbacid, 2005).

We and others have recently demonstrated that cyclin-dependent kinases (CDKs), key regulators of cell cycle progression and cell proliferation (Murray, 2004), participate in the regulation of metabolic pathways and energy homeostasis (Lopez-Mejia et al., 2018). CDK4 promotes adipocyte differentiation (Lagarrigue et al., 2016), and a mouse model of *cdk4* invalidation has increased oxidative metabolism and exercise capacity (Lopez-Mejia et al., 2017). Furthermore, the CDKs target (the retinoblastoma protein, pRB) and downstream effector E2F1 are both directly involved in the BAT activity in response to cold. At basal conditions, the complex pRb-E2F1 sits in the promoters of genes involved in oxidative metabolism and mitochondrial biogenesis, such as PGC1α, and inhibits their transcription BAT. In response to cold, pRB is

[1]Center for Integrative Genomics, University of Lausanne, Lausanne, Switzerland

[2]College of Animal Science and Technology, Northwest A&F University, Yangling, Shaanxi, China

[3]Institut National de la Santé et de la Recherche Médicale (Inserm), UMR1048, Institute of Metabolic and Cardiovascular Diseases, Toulouse, France

[4]Institut National de la Santé et de la Recherche Médicale (Inserm), Languedoc Roussillon, France

[5]These authors contributed equally

[6]Lead Contact

*Correspondence: lluis.fajas@unil.ch

https://doi.org/10.1016/j.isci.2020.101163

phosphorylated releasing this repression. Consequently, mice invalidated for E2f1 show higher body temperature upon cold stimulation due to increased oxidative metabolism (Blanchet et al., 2011).

CDK7 and its partners, cyclin H and MAT1, were originally isolated as a CDK-activating kinase (CAK), which was required for full activation of cell-cycle CDKs (Makela et al., 1994; Yee et al., 1995). CDK7 also phosphorylates the RNA polymerase II (Pol II) C-terminal domain (CTD), which initiates transcription (Shiekhattar et al., 1995). Based on this property, the inhibition of CDK7 with small molecules THZ1 has been considered a promising therapy for cancer (Glover-Cutter et al., 2009; Chipumuro et al., 2014; Christensen et al., 2014; Kwiatkowski et al., 2014; Nilson et al., 2015). The mouse model of CDK7 deficiency shows early embryonic lethality, which indicates its importance in development (Ganuza et al., 2012). With heart-specific knockout mice, CDK7/MAT1 complex has been implicated in controlling mitochondrial metabolism gene expression in heart and is important to prevent heart failure (Sano et al., 2007). Since CDK7 is an upstream regulator of the CDK-E2F1-RB pathway, and since these proteins are important modulators of BAT activity, we hypothesized that CDK7 could also be an important regulator of thermogenesis in adipose tissue.

In this study, we show, by analyzing the BAT and white adipose tissue (WAT)-specific $Cdk7^{bKO}$ and $Cdk7^{aKO}$ mice, that CDK7 is essential for brown adipose tissue-mediated non-shivering thermogenesis and that CDK7 ablation attenuates beta-adrenergic signaling in brown and beige adipose tissue. In conclusion, CDK7 is an important regulator of beta-adrenergic receptor signaling in thermogenic fat.

RESULTS

CDK7 Brown Fat-Specific Knockout Mice Are Cold Intolerant

To analyze the role of CDK7 specifically in brown adipose tissue, $Cdk7^{fl/fl}$ mice were crossed with mice expressing the Cre recombinase under the *Ucp*1 promoter to generate the brown adipose tissue-specific $Cdk7^{bKO}$. This resulted in the specific disruption of CDK7 mRNA expression in BAT, whereas the expression of *Cdk7* remains intact in both subcutaneous (scWAT) and perigonadal (pgWAT) and other tissues like liver, brain, and muscle (Figure S1A). $Cdk7^{fl/fl}$ and $Cdk7^{bKO}$ mice had similar body weight and fat/lean mass ratio (Figures 1A–1C). The food intake was indistinguishable between the two groups, as it was the activity at room temperature (Figures S2A and S2B). Not surprisingly, $Cdk7^{bKO}$ mice did not demonstrate any difference in glucose tolerance or insulin sensitivity (Figures S2C and S2D).

To explore the role of CDK7 in thermogenic regulation, $Cdk7^{bKO}$ and $Cdk7^{fl/fl}$ control littermates were challenged to acute cold exposure (4°C) and rectal temperatures were monitored. We found that, when food was removed during cold exposure at 4°C, $Cdk7^{bKO}$ mice developed severe hypothermia (body temperature <30°C) within 3 h, whereas $Cdk7^{fl/fl}$ mice kept the body temperature over 32°C, indicating that $Cdk7^{bKO}$ mice were cold intolerant (Figure 1D). Interestingly, when mice had free access to food during the cold exposure, $Cdk7^{bKO}$ was able to maintain the body temperature to a similar level as that of the $Cdk7^{fl/fl}$ mice (Figure S3A).

To further examine the requirement for CDK7 in regulating BAT function, we next measured whole-body O_2 consumption after acute β3-adrenergic stimulation in anesthetized mice. Although $Cdk7^{bKO}$ and control littermates showed similar O_2 consumption rates at the baseline, the increased O_2 consumption and energy expenditure triggered by the specific β3-adrenergic receptor agonist CL-316,243 (CL) that was observed in $Cdk7^{fl/fl}$ mice were blunted in the $Cdk7^{bKO}$ littermates, which suggested a deficient function of the BAT CDK7 in these mice (Figure 1E). We did not observe any differences in the respiratory exchange ratio (RER), which suggested no differences in substrate utilization (Figure 1F).

CDK7 Invalidation Leads to Interscapular BAT Atrophy and Impaired UCP1 Expression

We first observed that the interscapular BAT of $Cdk7^{bKO}$ mice weighted 60% less than the BAT of control littermates (Figures 2A and 2B). Histologic analysis of BAT sections from $Cdk7^{bKO}$ mice were heterogeneous in cell size, some adipocytes having increased unilocular lipid droplets and other cells without lipid droplets. In addition, we observed exacerbated eosinophilic (red) staining (Figure 2C), which indicated an increase in immune cell infiltration in the BAT of the $Cdk7^{bKO}$ mice.

BAT thermogenesis is mediated by UCP1. We therefore checked its expression in our mouse model to elucidate the molecular basis through which CDK7 controls BAT thermogenesis. Western blotting result

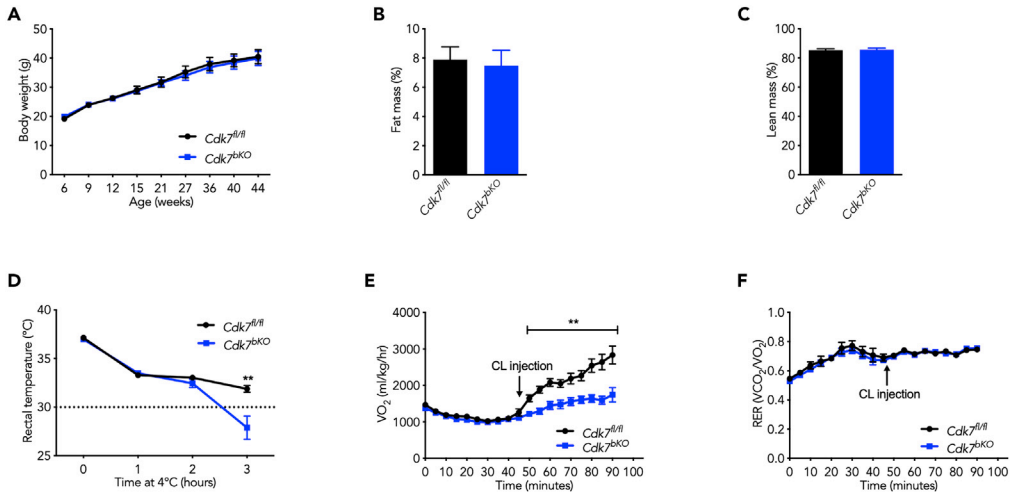

Figure 1. CDK7 Brown Fat-Specific Knockout Mice Are Cold Intolerant

(A) Weight gain of male littermates fed chow diet (CD) was recorded (n = 10 for each group).

(B) Fat mass were analyzed by EchoMRI (8-weeks-old male, n = 10 for each group). (C) Lean mass were analyzed by EchoMRI (8-weeks-old male, n = 10 for each group)

(D) Acute cold response of *Cdk7*^{bKO} and control littermates was performed without food supply to evaluate thermogenic activity in control and *Cdk7*^{bKO} mice (male, 6–8 weeks, n = 8 for each group).

(E and F) Loss of CDK7 in BAT leads to a reduced response to acute β3-adrenergic signaling. Mice were anesthetized with pentobarbital and put in the individual chambers at 33°C for basal measurement; after the measurement was stable, CL-316,243 (100 μg/kg) was injected at time indicated by arrows as described in Transparent Methods. Oxygen consumption (E) was measured from a comprehensive laboratory animal monitoring system (CLAMS). (F) The respiratory exchange ratio (RER) is calculated as the ratio between VCO_2 and VO_2 (male, 8–9 weeks, n = 7–8 for each group).

Values represent means ± SEM. **p < 0.01. See also Figures S1 and S2.

revealed that the expression of both UCP1 and PGC1α was decreased in *Cdk7*^{bKO} BAT harvested at room temperature (Figure 2D and 2E), which was consistent with immunohistochemical analysis (Figure 2F).

CDK7 Is Required for the Induction of Genes Involved in the Thermogenic and Inflammatory Responses to Cold

To have a global view of the genes that are affected by CDK7 depletion in BAT, we next performed RNA sequencing (RNA-seq) on BAT from control and *Cdk7*^{bKO} mice at room temperature or after 6 h of cold exposure with free access to food. Principal-component analysis (PCA) analysis showed a good separation of genotypes and treatments (Figure 3A). Applying cutoffs of a significance level of false discovery rate (FDR) <0.05, the expression of 1,197 was induced after 6 h cold exposure compared with room temperature conditions in the control group. In contrast, the number of genes whose expression was induced by cold in *Cdk7*^{bKO} mice was only 268 (Figure 3B). Strikingly, only 148 of the 1,197 genes induced by cold exposure in WT mice were significantly induced in *Cdk7*^{bKO} BAT, showing that CDK7 is required for the vast majority (87%) of the transcriptional adaptation to acute cold stimulation. On the other hand, in basal conditions at room temperature, 876 genes showed reduced expression in *Cdk7*^{bKO} BAT compared with control BAT. Under cold conditions, the expression of 1,382 genes was decreased in *Cdk7*^{bKO} BAT compared with control BAT.

The differentially expressed genes in BAT between genotypes was evaluated by GO enrichment analysis. Both at room temperature and upon cold exposure, genes down-regulated in the *Cdk7*^{bKO} BAT was enriched in mitochondrial and energy metabolism (Figures 3D and 3E). Moreover, decreased thermogenic genes in response to cold, like UCP1, PGC1α, and DIO2, was confirmed by qPCR and revealed by heatmap (Figures 3F and 3G). On the other hand, genes up-regulated in the same conditions in the *Cdk7*^{bKO} BAT, compared with the BAT of control mice, were enriched in the inflammation response-related GOs, such as cytokine production (Figures 3F and 3G). Moreover, the expression of these inflammation-related genes, like the macrophage markers F4/80 and the cytokine TNF-α, were confirmed by qPCR (Figure 3H).

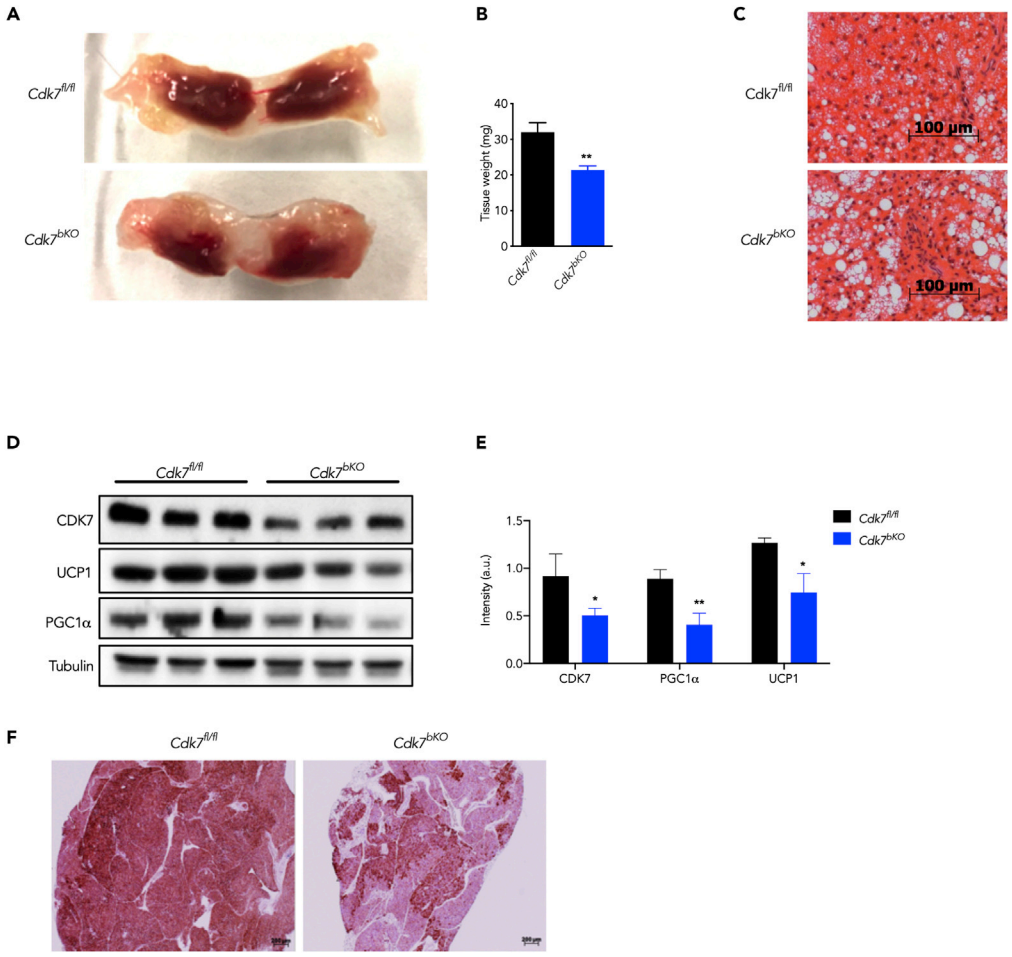

Figure 2. CDK7 Ablation Leads to Interscapular BAT Atrophy and Impaired UCP1 Expression

(A) Brown adipose tissue (BAT) pictures from male control *Cdk7*$^{fl/fl}$ and *Cdk7*^{bKO} mice at room temperature (male, 12 weeks).

(B) Brown adipose tissue (BAT) weight from male control and *Cdk7*^{bKO} mice at room temperature (male, 12 weeks).

(C) Hematoxylin and eosin staining of BAT (scale bar, 100 μm).

(D) Western blot analyses of protein levels of CDK7, UCP1, and PGC1α in BAT. Tubulin was used as the loading control.

(E) Quantification of the intensity of the bands observed in (D).

(F) UCP1 immunostaining of BAT at room temperature.

Values represent means ± SEM. *p < 0.05,**p < 0.01. See also Figure S3.

Interestingly, RNA pol II phosphorylation was not changed in the BAT of the *Cdk7*^{bKO} mice, which suggested that the effects of CDK7 on gene transcription were independent of its function of regulating RNA pol II activity (Figure 3I). Taken together our data suggested that CDK7 is a critical regulator of brown fat thermogenesis and an inhibitor of adipose tissue inflammation.

Creatine Metabolism Compensates for the Impairment in UCP1-Mediated Thermogenesis in *Cdk7*^{bKO} Mice Fed *Ad Libitum*

Since "normal" animal housing conditions (20°C–25°C) represent a chronic mild thermal stress to mice, and our results demonstrated impaired brown adipose tissue function and thermogenesis in *Cdk7*^{bKO} mice, we examined the effect of CDK7 invalidation at thermoneutrality. We reasoned that, similar to UCP1 KO mice, *Cdk7*^{bKO} mice would become obese owing to the impairment of diet-induced thermogenesis. However, *Cdk7*^{bKO} did not develop obesity and showed unaltered oxygen consumption, energy expenditure, and food intake (Figures S4A–S4F). This suggested that *Cdk7*^{bKO} mice, when fed normal diet, developed a mechanism to compensate for the deficient UCP1-dependent energy dissipation in BAT.

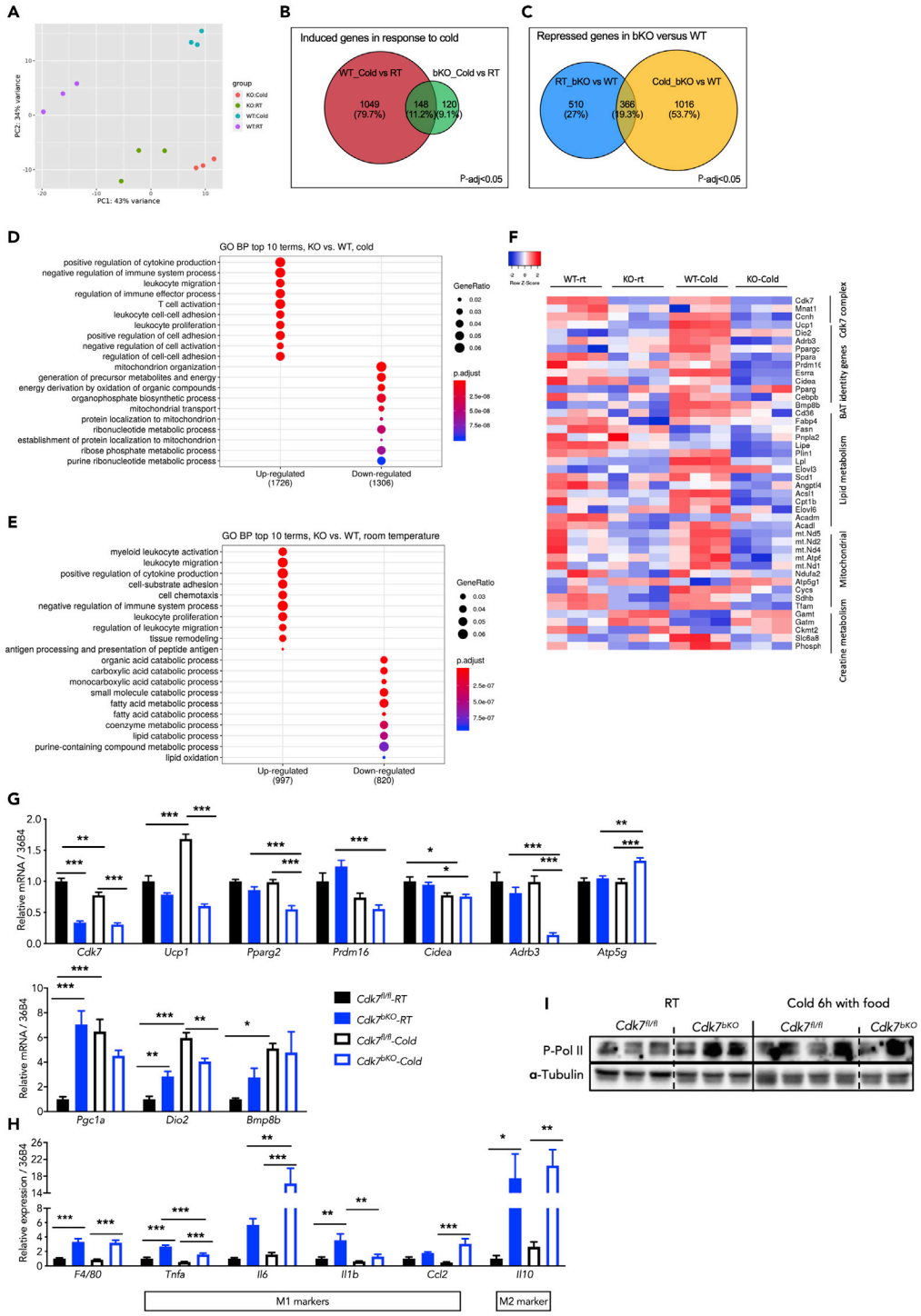

Figure 3. RNA Sequencing and qPCR Analyses of the BAT of *Cdk7*^{bKO} Mice

(A) PCA analysis was performed on the RNA-seq data of BAT of *Cdk7*^{bKO} mice and control in response to cold.

(B) Venn map showing the number of genes which expression is upregulated in the BAT at room temperature and in response to cold in *Cdk7*^{bKO} and *Cdk7*$^{fl/fl}$ mice (p-adj < 0.05 cutoff). (C) Venn map showing the number of genes which expression is downregulated in the BAT at room temperature and in response to cold in *Cdk7*^{bKO} and *Cdk7*$^{fl/fl}$ mice (p-adj < 0.05 cutoff).

(D and E) Enrichment of differentially expressed genes in the BAT of *Cdk7*^{bKO} versus *Cdk7*$^{fl/fl}$ mice in cold (D) or room temperature (E).

Figure 3. *Continued*

(F) Heatmap of RNA-seq analysis of gene expression in *Cdk7*^{bKO} and control littermates at room temperature and in response to cold.

(G) Quantitative PCR analysis of the expression of *Ucp1* and other BAT marker genes in response to cold (male, 12 weeks, n = 7 for each group).

(H) M1 and M2 macrophages markers were analyzed by qPCR.

(I) Western blot analysis of the expression of the phosphorylated RNA pol II.

Values represent means ± SEM. *p < 0.05, **p < 0.01, ***p < 0.001. See also Figure S3.

It has been reported that the creatine-driven substrate cycle enhances energy expenditure and thermogenesis in beige and brown fat. Furthermore, a genetic model of mouse with abrogated expression of the key creatine metabolism gene *Gatm* leads to impairment of diet-induced thermogenesis and mouse become obese. This study provides strong *in vivo* genetic support for a role of creatine metabolism in energy expenditure. Analysis of our RNA-seq data indicated increased expression of the rate-limiting enzymes of creatine biosynthesis (Figure 3F). These data were confirmed by qPCR analysis, showing higher expression levels of *Gatm*, *Gamt*, the creatine transporter *Slc6a8*, and the creatine kinase *Ckmt1* in *Cdk7*^{bKO} BAT, compared with *Cdk7*$^{fl/fl}$ control mice (Figure 4A). These results are in accordance with a compensation of the UCP1-driven thermogenesis impairment by creatine metabolism. To validate this hypothesis, we decided to inhibit creatine metabolism in *Cdk7*^{bKO} mice. The *Cdk7*^{bKO} and control littermates were daily intraperitoneally injected for 4 days during cold exposure with β-guanidinopropionic acid (β-GPA), a creatine analog that inhibits creatine transport and reduces creatine levels *in vivo*. We found no difference in body temperature during the first 2 days after β-GPA injection in both *Cdk7*^{bKO} mice or littermate controls. The body temperature of *Cdk7*^{bKO} mice were, however, significantly lower in mice treated with β-GPA, suggesting that, when UCP1 expression is impaired, creatine metabolism compensates for cold-induced thermogenesis in these mice (Figure 4C).

Adipose Tissue-Specific *Cdk7*^{aKO} Mice Have Impaired Response to β3-Adrenoceptor Agonist in White Adipose Tissue

Beige and brown fat share common features in terms of thermogenic properties (Ikeda et al., 2018). Since *Cdk7* ablation results in impaired BAT development and function, we wondered how CDK7 could affect white adipose tissue browning. We thus generated pan-adipose tissue-specific *Cdk7* knockout mice (*Cdk7*^{aKO}) using the *Adipoq* promoter-driven Cre recombinase transgenic mice (Figure S5). The BAT phenotype (in *Cdk7*^{aKO} mice, Figure S6) was similar with what we observed with *Cdk7*^{bKO}. Eight-week-old control or *Cdk7*^{aKO} mice were treated with the β3-adrenoceptor agonist CL-316,243 or an equivalent volume of sterile saline for 7 days. *Cdk7*$^{fl/fl}$ control mice exhibited intensive CL-induced browning in scWAT assessed by the appearance of multilocular lipid droplets (Figure 5A). However, this typical feature of beige in CL-316,243-treated *Cdk7*^{aKO} scWAT was less intense compared with *Cdk7*$^{fl/fl}$ control mice (Figure 5A). In pgWAT of control mice, the browning effect of CL-316,243 was milder (Figure 5B), but in the pgWAT of the *Cdk7*^{aKO} mice larger adipocytes were found together with infiltrating non-adipocyte cells. The expression of thermogenesis-related genes in scWAT and pgWAT of control *Cdk7*$^{fl/fl}$ mice were increased in response to CL-316,243 treatment, whereas *Cdk7*^{aKO} mice did not increase the expression of these genes in the same WAT depots (Figures 5C–5E), which was consistent with the observed morphological changes (Figures 5A and 5B).

Interestingly, the histology of the pgWAT in *Cdk7*^{aKO} mice treated with CL-316,243 resembled an exacerbated inflammatory response (Figure 5B). Indeed, F4/80 immunostaining confirmed a strong macrophage infiltration (Figure 5H). Moreover, mRNA expression analysis showed a significant increase in F4/80, IL-6, and TNF-α genes in response to CL-316,243 treatment in pgWAT but not in scWAT (Figures 5F and 5G). Together, these data indicated that CDK7 is required for the β3-adrenoceptorinduced white adipose tissue browning and that CDK7 ablation triggers an immune response in pgWAT in response to β3-adrenoceptor stimulation.

Induction of the β3-Adrenergic Pathway Triggers a Similar Gene Expression Pattern in the *Cdk7*^{bKO} BAT and *Cdk7*^{aKO} WAT

To identify the specific pathways that CDK7 regulates in WAT, we next performed RNA-seq on pgWAT after 7 days saline or CL-316,243 treatment. PCA analysis result showed a good separation of genotypes and treatments. We did not observe major difference between *Cdk7*^{aKO} and *Cdk7*$^{fl/fl}$ mice when we analyzed

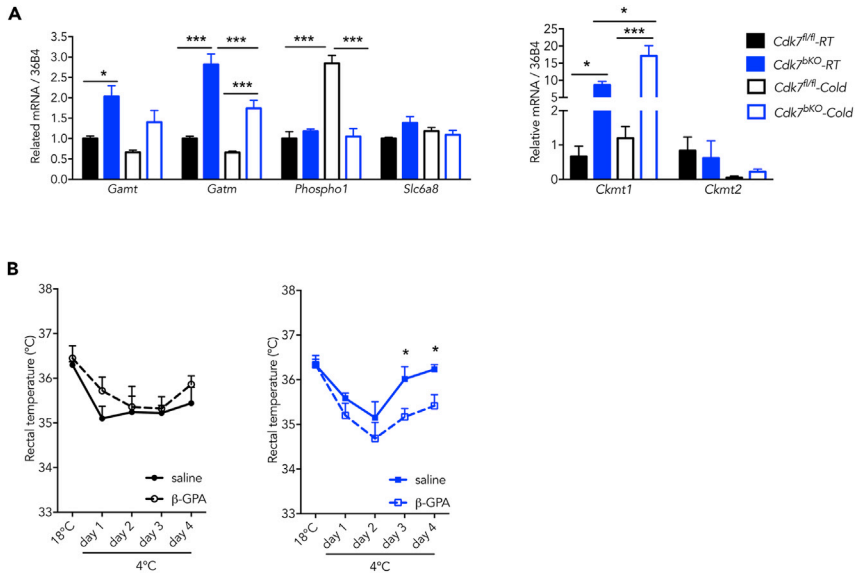

Figure 4. Creatine Metabolism Can Compensate for Impairment of UCP1-Mediated Thermogenesis

(A) Creatine metabolism-related genes were analyzed by qPCR in *Cdk7*^{bKO} BAT compared with control *Cdk7*$^{fl/fl}$ littermates.

(B) Body temperature of *Cdk7*$^{fl/fl}$ and *Cdk7*^{bKO} mice treated with vehicle or β-GPA (0.4 g/kg); (n = 5–6 mice per group). All values represent means ± SEM. *p < 0.05, ***p < 0.001. See also Figure S4.

the global gene expression in the WAT. In contrast, the CL-316,243 clearly separated in different clusters both genotypes, indicating significant differences in the global gene expression (Figures 6A and 6B).

We next performed a cross analysis between the RNA-seq data that we obtained for the BAT of the *Cdk7*^{bKO} and *Cdk7*$^{fl/fl}$ in response to cold (Figure 3) and the data of the WAT analysis in *Cdk7*^{aKO} and *Cdk7*$^{fl/fl}$ mice (Figures 6A and 6B). We focused on the genes that were commonly up- or down-regulated in the WAT and BAT in response to β3-adrenergic stimulation (CL-316,243 treatment in WAT, and cold in BAT). The Venn diagrams showed that 163 genes were commonly upregulated and 156 genes were inhibited in the intersection of the two datasets (Figure 6C). The GO Biological Process analysis for the 163 up- and 156 down-regulated genes indicated that the immune response-related pathways were the most representatives in the up-regulated genes. The main down-regulated pathways were fat metabolism, mitochondrial and thermogenic groups (Figure 6D and Table S1). These results were consistent with the phenotype of both the *Cdk7*^{aKO} and *Cdk7*^{bKO} mice.

DISCUSSION

We prove here that *Cdk7* knockout leads to BAT atrophy, with a consistent decrease in UCP1 expression as well as the expression of oxidative and thermogenic genes in response to cold. Consequently, *Cdk7*^{bKO} mice are cold intolerant. The thermogenic property of brown and beige adipocytes can transform stored energy into heat; thus, the manipulation of their activity is a potential therapeutic target to treat obesity and type 2 diabetes (Kajimura et al., 2015). However, the impaired thermogenic function does not necessarily lead to metabolic dysfunction. *Cdk7*^{bKO} mice, despite the atrophy of BAT and beige WAT are metabolically normal. This finding is reminiscent of mice lacking ERRγ in BAT. ERRγ preserves brown fat innate thermogenic activity at thermoneutrality. Similar to *Cdk7*^{bKO} mice, ERRγ KO mice do not gain more weight than WT mice despite a severely blunted thermogenic capacity (Ahmadian et al., 2018). Moreover, mice with depleted expression of the master regulator of thermogenesis, UCP1, are resistant to diet-induced obesity, which suggests that some compensatory mechanisms take over the energy dissipation processes (Enerback et al., 1997; Liu et al., 2003).We found that in the *Cdk7*^{bKO} mice the lack of a metabolic phenotype was explained by a compensatory increase in the expression of genes related to the creatine metabolism. Furthermore, the pharmacological reduction of creatine levels in the *Cdk7*^{bKO} mice reduces the core body temperature in response to cold. Indeed, a mitochondrial substrate cycle was found to be regulated by creatine to drive thermogenesis (Bertholet et al., 2017; Kazak et al., 2015). The creatine cycle can only generate

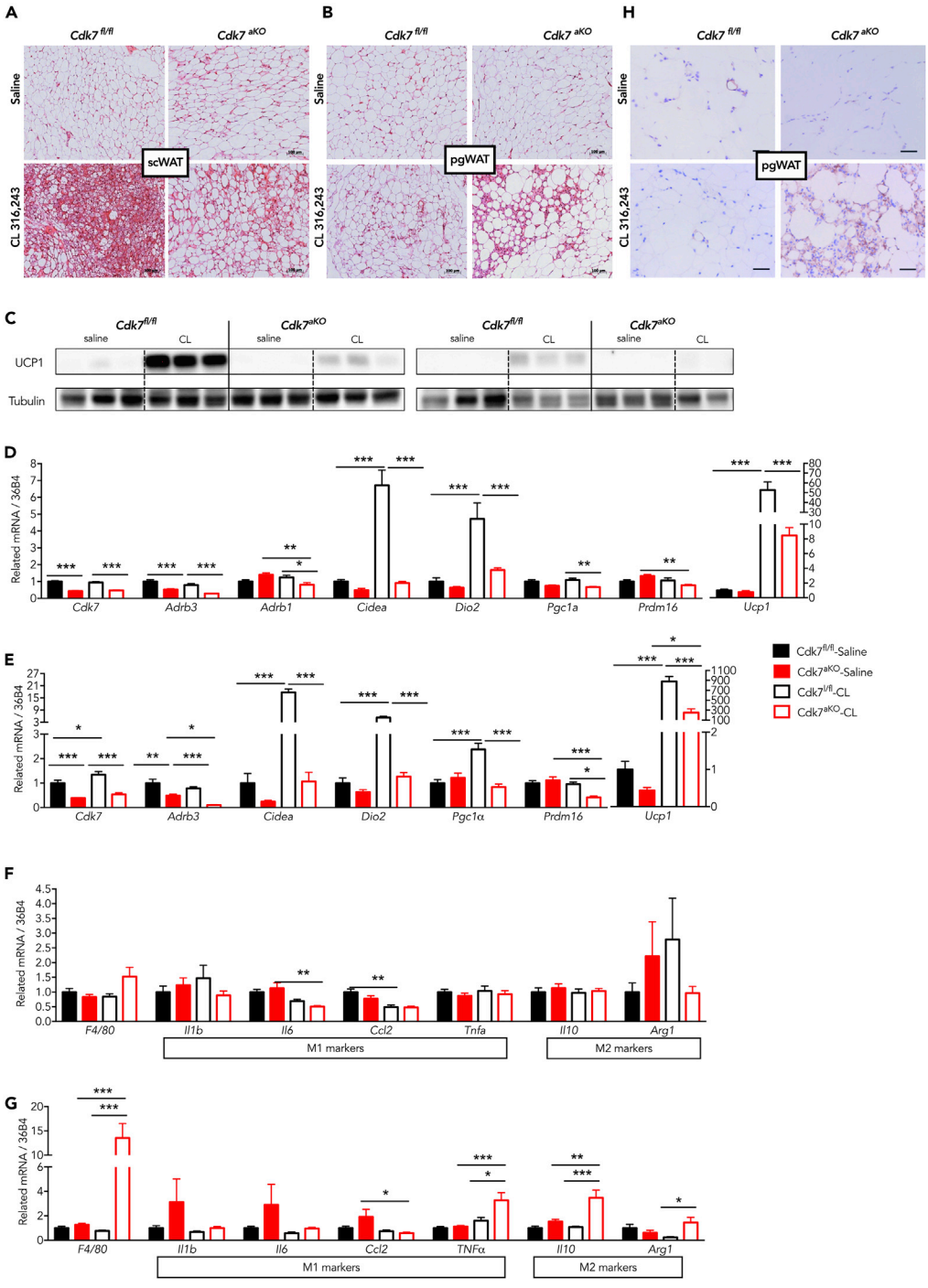

Figure 5. *Cdk7*^{aKO} Mice Have Decreased Response to β3 Adrenoceptor Agonist-Induced White Adipose Tissue Browning

(A) H&E staining of scWAT of *Cdk7*^{aKO} and control littermates after 7 days treatment with CL or equal amount of saline. (B) H&E staining of pgWAT of *Cdk7*^{aKO} and control littermates after 7 days treatment with CL or equal amount of saline.

(C) UCP1 protein level in scWAT (left) and pgWAT (right) of *Cdk7*^{aKO} and control littermates were detected by western blotting.

(D) Browning-related genes in scWAT were detected by qPCR. (E) Browning-related genes in pgWAT were detected by qPCR.

Figure 5. *Continued*

(F) M1 and M2 macrophages markers in scWAT were analyzed by qPCR. (G) M1 and M2 macrophages markers in pgWAT were analyzed by qPCR.

(H) F4/80 immunostaining of pgWAT of $Cdk7^{aKO}$ and control mice after 7 days treatment with CL or equal amount of saline. (male, 8–9 mice for each group; scale bar, 50 μm).

Values represent means ± SEM. *p < 0.05, **p < 0.01, ***p < 0.001. See also Figures S5 and S6.

heat under nutrient availability conditions, whereas under fasting conditions, the creatine cycle cannot compensate. Interestingly, the thermogenic phenotype in the $Cdk7^{bKO}$ mice was only apparent under fasting conditions, suggesting that the creatine compensatory mechanism is responsible for the slow modulation of the metabolic rate but not for fasting adaptive thermogenesis in brown fat in these mice.

The role of CDK7 in adipose tissue biology was not limited to the regulation of BAT function. We show that CDK7 is also required for the β3-adrenergic induced browning of WAT. CDK7 ablation in whole adipose tissue demonstrated reduced expression of oxidative and thermogenic genes after long-term CL-316,243 injection. CDK7 is therefore in the intersection between BAT and WAT biology as a mediator of the β-adrenergic signaling in these tissues. Most interesting, we found that CDK7 ablation triggers an immune reaction in BAT in response to cold and in pgWAT in response to adrenergic stimulation. When we crossed the RNA-seq data in the $Cdk7^{bKO}$ and $Cdk7^{aKO}$ mice we evidenced that targeting CDK7 in BAT or WAT causes a cellular increase in the expression of pro-inflammatory cytokines/chemokines in both tissues. Genes involved in the immune response were indeed the first class of genes that were upregulated in the absence of CDK7 both in BAT and in WAT. F4/80 staining confirmed increased macrophage infiltration in both BAT and pgWAT upon CDK7 ablation. In support of our findings is a very recent publication by the group of Wong who demonstrated that CDK7 inhibition using a specific molecule potentiated anti-tumor immunity (Zhang et al., 2020). They showed that the blockade of the activity of CDK1 and CDK2, as a result of CDK7 inhibition, induced DNA replication stress and genome instability, which ultimately triggered the immune response. The resulting phenotype of CDK7 inhibition, i.e., the exacerbated immune response, is similar to the inflammatory reaction that we observed in the adipose tissues of WAT and BAT-specific CDK7 KO mice. Moreover, RNA-seq analysis showed that the major class of genes that were induced by CDK7 inhibition or deletion belonged to the immune response GO in both the cancer and the adipose models. The CDK7-mediated mechanisms that trigger the immune response in BAT and in cancer cells are, however, different. CDK7 functions as both a CAK and TFIIH associated kinase. The CAK function of CDK7 was directly involved in the above-mentioned study in the lung cancer cells (Zhang et al., 2020), whereas this is not likely the mechanism in BAT. Two arguments support this hypothesis. First, in our model, *Cdk7* is ablated in mature brown adipocyte, which is considered post mitotic and exempt from cell cycle. Second, another potential CDK7 (CAK) target, CDK6, negatively regulates white fat browning (Hou et al., 2018), which is opposite to our findings with CDK7. Moreover, we show in an independent study (unpublished, in revision) that CDK4, which is a downstream effector of CDK7, has an opposite function in BAT. $Cdk4^{-/-}$ mice, opposite to *Cdk7* knockout mice, have increased BAT activity, proving that the CAK function of CDK7 in thermogenic fat is dispensable.

Upon cold exposure, mice typically increase lipid droplets in BAT, indicative of increased lipogenesis. Cold stimulates the simultaneous induction of fatty acid synthesis and β-oxidation to facilitate both mitochondrial heat production and to preserve a pool of fatty acids (Yu et al., 2002; Sanchez-Gurmaches et al., 2018). Interestingly, the BAT from $Cdk7^{bKO}$ mice were delipidated after cold exposure (Figure S3B). Delipidation could be caused, at least in part, by a high ratio of lipolysis, since we observed an increase in the phosphorylation of hormone-sensitive lipase (HSL) at serine 660, which is a marker of active lipolysis. $Cdk7^{bKO}$ mice may upregulate lipolysis as a compensatory mechanism for their defective thermogenic program (Schreiber et al., 2017; Shin et al., 2017). Moreover, the increased lipolysis and accumulation of free fatty acid could lead to the inflammatory response that we observed in both BAT and pgWAT (Mottillo et al., 2010).

As a component of TFIIH, CDK7 can phosphorylate the RNA polymerase II to regulate transcription. The first characterization of the $Cdk7^{-/-}$ mice showed, however, that this function is dispensable and can be compensated by other kinases (Ganuza et al., 2012). Our results were consistent with these findings. Indeed, phosphorylation of RNA polymerase II was not different between WT and $Cdk7^{bKO}$ BAT, which suggested other kinases compensate for the role of CDK7 in transcription initiation also in BAT. Taken together, our data proved that the function of CDK7 in BAT was beyond its canonical role as a CAK or a general transcriptional regulator.

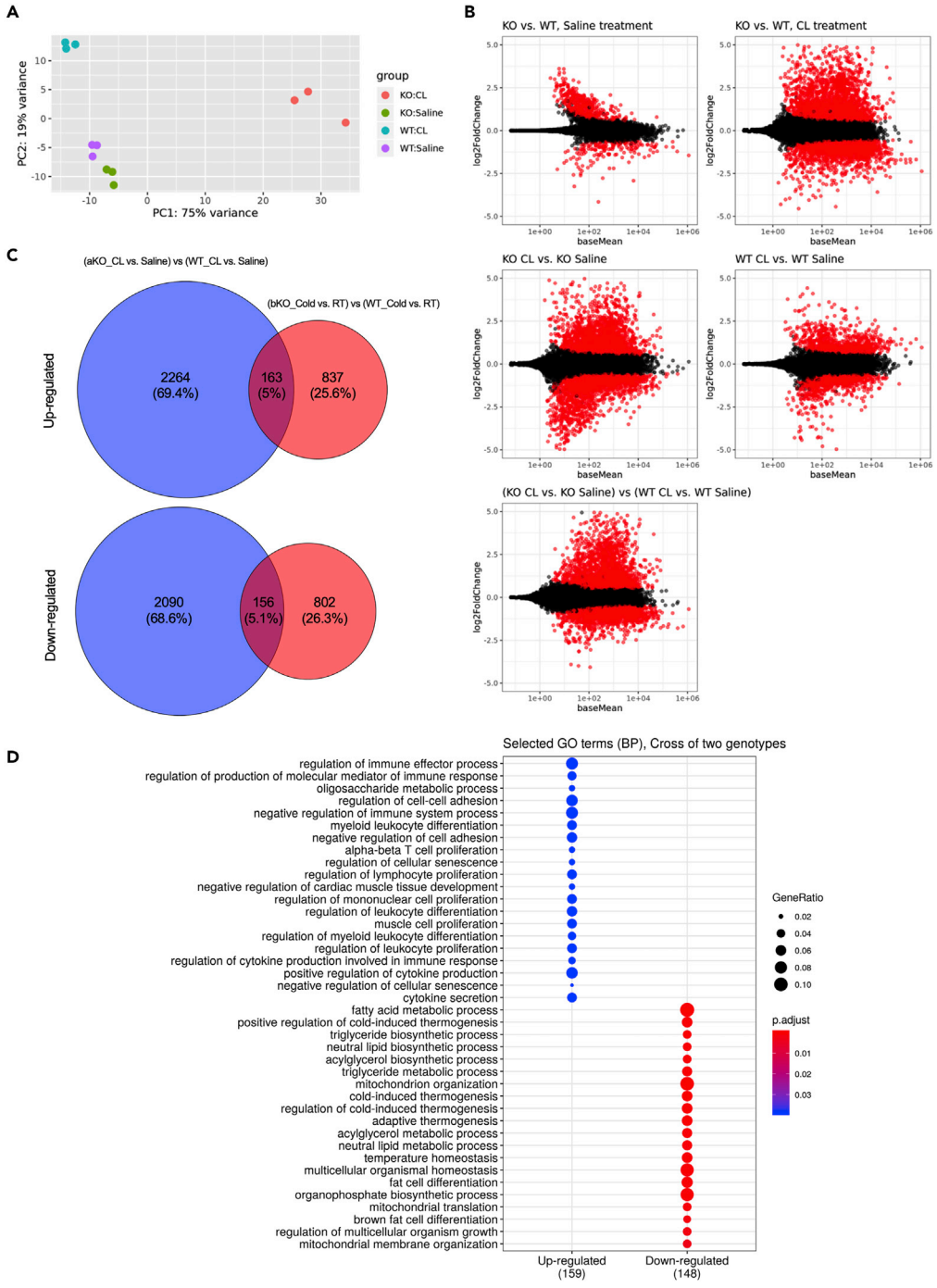

Figure 6. Converging Gene Expression Pattern in *Cdk7*^{aKO} and *Cdk7*^{bKO} Mice

(A) PCA analysis was performed on the RNA-seq data of pgWAT of *Cdk7*^{aKO} and *Cdk7*$^{fl/fl}$ mice in response to CL treatment.

(B) The plot of the differentially expressed gene number in pgWAT of *Cdk7*^{aKO} mice by different comparisons.

(C) Venn map showing the number of differentially expressed genes in pgWAT of *Cdk7*^{aKO} mice and BAT of *Cdk7*^{bKO} mice, with the cutoff of p value (FDR adjusted) < 0.05 and $|log_2FC| > 0.5$.

(D) Enrichment of the differentially expressed genes of the intersection genes list in (C).

See also Table S1.

CDK7 is an emerging target for cancer therapy. CDK7 inhibitors are efficient in the treatment of several models of cancers, including, but not limited to, the lung, breast, prostate, and ovarian tumors (Sun et al., 2020; Rasool et al., 2019; Kim et al., 2020; Zhang et al., 2020). In our study we show that, in addition to the canonical effects in gene transcription and cell cycle control, CDK7 also regulates the activity of BAT and WAT in response to cold and adrenergic stimulation. Strikingly, BAT activity has been related to cachexia, which is a wasting syndrome suffered by about half of patients with cancer. Cachexia is characterized by high energy expenditure in adipose tissue and skeletal muscle and increased thermogenesis in BAT (Bianchi et al., 1989; Shellock et al., 1986). The mechanisms by which tumors induce thermogenesis in BAT are not fully understood, although the tumor-derived signaling through the parathyroid-hormone-related protein could explain it (Kir et al., 2014). From our results we can expect that the treatment with CDK7 inhibitors will block the activity of BAT and therefore improve cachexia in patients with cancer.

In conclusion, by combining CDK7 BAT-specific and pan-AT-specific knockout mice model, we demonstrated that CDK7 is an important mediator of β3-adrenergic signaling pathways under catabolic conditions in thermogenic brown and beige fat.

Limitations of the Study

Our study proves that CDK7 regulates BAT activity as well as WAT browning in a cell-cycle-independent manner. We also provide evidence that CDK7 is essential for beta-adrenergic signaling in thermogenic fat. However, further experiments, including phospho-proteomics and *in vitro* kinase assays, should be employed to identify the targets of CDK7 that mediate the observed effects. These potential targets may include but are not limited to key thermogenic transcriptional factors and possible direct targets on beta-adrenergic signaling pathway. In addition, we found that the compensation by the creatine futile cycle in CDK7 knockout BAT leads to resistance to metabolic dysfunction. Further analyses of metabolites (e.g., creatine, phosphocreatine, ATP, ADP) levels under different conditions (like cold/thermoneutrality, fast/fed) in CDK7 knockout BAT and control will be helpful to decipher the reciprocal relationship of CDK7 knockout and creatine metabolism.

In addition to the effects of CDK7 in fully differentiated BAT cells, as is shown in this study, we cannot exclude the possibility that CDK7 is also involved in adipocyte differentiation. Specific knockout of CDK7 in the progenitors of brown fat with Myf5-cre during BAT development can be employed to answer this question.

Last but not least, CDK7 ablation triggers immune response in brown adipose tissue and also after CL induced browning in pgWAT. Further experiments need to be done to identify which signal or adipokine secretion could be altered that leads to this immune response, as our mice models are adipocyte specific and any non-adipocyte-related phenotype should originate from adipocyte dysfunction.

Resource Availability

Lead Contact

Further information and requests for resources and reagents should be directed to and will be fulfilled by Lluis Fajas (lluis.fajas@unil.ch).

Materials Availability

All unique/stable reagents generated in this study are available from the Lead Contact with a completed Materials Transfer Agreement.

Data and Code Availability

The datasets/code generated during this study are available at GEO accession GSE149128: https://www.ncbi.nlm.nih.gov/geo/query/acc.cgi?acc=GSE149128. Enter token uvmpyysixtalxwl into the box.

The original data sources are available in Mendeley Data DOI 10.17632/cvmzwtd4vj.2.

METHODS

All methods can be found in the accompanying Transparent Methods supplemental file.

SUPPLEMENTAL INFORMATION

Supplemental Information can be found online at https://doi.org/10.1016/j.isci.2020.101163.

ACKNOWLEDGMENTS

The authors acknowledge all the members of the Fajas laboratory for support and discussions. The authors thank Sandra Calderon, Johann Weber, and Hannes Richter from Lausanne Genomic Technologies Facility for RNA sequencing sample preparation and data analysis. We also thank Frederic Preitner and Gilles Willemin from Mouse Metabolic Facility of CIG (University of Lausanne, Switzerland) for experimental assistance. We thank M. Barbacid and D. Santamaria (CNIO, Spain) for providing the Cdk7 flox mice. H.J. and Y.C. are supported by scholarship (No.201406300121 and No.201706300109) from China Scholarship Council. This work from Prof. Fajas lab is supported by the Swiss National Foundation (31003A_143369). The authors thank Prof. Francesc Villarroya, Prof. Dario Diviani, Prof. Kei Sakamoto, and Dr Jean-Sébastien Annicotte for helpful discussion.

AUTHOR CONTRIBUTIONS

L.F. designed the study. H.J. and Y.C. performed most experiments, with assistance from J.C.-A., I.C.L.-M., B.D., and P.-D.D. R.D. performed bioinformatics analysis. C.M. performed histology staining. G.N. participated in the mouse experiment. H.J., Y.C., and L.F. wrote the manuscript. All authors read and provided comments on the manuscript.

DECLARATION OF INTERESTS

The authors declare no competing interests.

Received: February 3, 2020
Revised: March 31, 2020
Accepted: May 11, 2020
Published: June 26, 2020

REFERENCES

Ahmadian, M., Liu, S., Reilly, S.M., Hah, N., Fan, W., Yoshihara, E., Jha, P., De Magalhaes Filho, C.D., Jacinto, S., Gomez, A.V., et al. (2018). ERRgamma preserves Brown fat innate thermogenic activity. Cell Rep. *22*, 2849–2859.

Bertholet, A.M., Kazak, L., Chouchani, E.T., Bogaczynska, M.G., Paranjpe, I., Wainwright, G.L., Betourne, A., Kajimura, S., Spiegelman, B.M., and Kirichok, Y. (2017). Mitochondrial patch clamp of beige adipocytes reveals UCP1-positive and UCP1-negative cells both exhibiting futile creatine cycling. Cell Metab. *25*, 811–822 e4.

Bianchi, A., Bruce, J., Cooper, A.L., Childs, C., Kohli, M., Morris, I.D., Morris-Jones, P., and Rothwell, N.J. (1989). Increased brown adipose tissue activity in children with malignant disease. Horm. Metab. Res. *21*, 640–641.

Blanchet, E., Annicotte, J.S., Lagarrigue, S., Aguilar, V., Clape, C., Chavey, C., Fritz, V., Casas, F., Apparailly, F., Auwerx, J., and Fajas, L. (2011). E2F transcription factor-1 regulates oxidative metabolism. Nat. Cell Biol. *13*, 1146–1152.

Cannon, B., and Nedergaard, J. (2004). Brown adipose tissue: function and physiological significance. Physiol. Rev. *84*, 277–359.

Chipumuro, E., Marco, E., Christensen, C.L., Kwiatkowski, N., Zhang, T., Hatheway, C.M., Abraham, B.J., Sharma, B., Yeung, C., Altabef, A., et al. (2014). CDK7 inhibition suppresses super-enhancer-linked oncogenic transcription in MYCN-driven cancer. Cell *159*, 1126–1139.

Christensen, C.L., Kwiatkowski, N., Abraham, B.J., Carretero, J., Al-Shahrour, F., Zhang, T., Chipumuro, E., Herter-Sprie, G.S., Akbay, E.A., Altabef, A., et al. (2014). Targeting transcriptional addictions in small cell lung cancer with a covalent CDK7 inhibitor. Cancer Cell *26*, 909–922.

Enerback, S., Jacobsson, A., Simpson, E.M., Guerra, C., Yamashita, H., Harper, M.E., and Kozak, L.P. (1997). Mice lacking mitochondrial uncoupling protein are cold-sensitive but not obese. Nature *387*, 90–94.

Fedorenko, A., Lishko, P.V., and Kirichok, Y. (2012). Mechanism of fatty-acid-dependent UCP1 uncoupling in brown fat mitochondria. Cell *151*, 400–413.

Ganuza, M., Saiz-Ladera, C., Canamero, M., Gomez, G., Schneider, R., Blasco, M.A., Pisano, D., Paramio, J.M., Santamaria, D., and Barbacid, M. (2012). Genetic inactivation of Cdk7 leads to cell cycle arrest and induces premature aging due to adult stem cell exhaustion. EMBO J. *31*, 2498–2510.

Glover-Cutter, K., Larochelle, S., Erickson, B., Zhang, C., Shokat, K., Fisher, R.P., and Bentley, D.L. (2009). TFIIH-associated Cdk7 kinase functions in phosphorylation of C-terminal domain Ser7 residues, promoter-proximal pausing, and termination by RNA polymerase II. Mol. Cell. Biol. *29*, 5455–5464.

Granneman, J.G., Burnazi, M., Zhu, Z., and Schwamb, L.A. (2003). White adipose tissue contributes to UCP1-independent thermogenesis. Am. J. Physiol. Endocrinol. Metab. *285*, E1230–E1236.

Hou, X., Zhang, Y., Li, W., Hu, A.J., Luo, C., Zhou, W., Hu, J.K., Daniele, S.G., Wang, J., Sheng, J., et al. (2018). CDK6 inhibits white to beige fat transition by suppressing RUNX1. Nat. Commun. *9*, 1023.

Ikeda, K., Kang, Q., Yoneshiro, T., Camporez, J.P., Maki, H., Homma, M., Shinoda, K., Chen, Y., Lu, X., Maretich, P., et al. (2017). UCP1-independent signaling involving SERCA2b-mediated calcium cycling regulates beige fat thermogenesis and systemic glucose homeostasis. Nat. Med. *23*, 1454–1465.

Ikeda, K., Maretich, P., and Kajimura, S. (2018). The common and distinct features of Brown and beige adipocytes. Trends Endocrinol. Metab. *29*, 191–200.

Kajimura, S., Spiegelman, B.M., and Seale, P. (2015). Brown and beige fat: physiological roles beyond heat generation. Cell Metab. *22*, 546–559.

Kazak, L., Chouchani, E.T., Jedrychowski, M.P., Erickson, B.K., Shinoda, K., Cohen, P., Vetrivelan, R., Lu, G.Z., Laznik-Bogoslavski, D., Hasenfuss, S.C., et al. (2015). A creatine-driven substrate cycle enhances energy expenditure and thermogenesis in beige fat. Cell *163*, 643–655.

Kazak, L., Chouchani, E.T., Lu, G.Z., Jedrychowski, M.P., Bare, C.J., Mina, A.I., Kumari, M., Zhang, S., Vuckovic, I., Laznik-Bogoslavski, D., et al. (2017). Genetic depletion of adipocyte creatine metabolism inhibits diet-induced thermogenesis and drives obesity. Cell Metab. *26*, 660–671.e3.

Kazak, L., Rahbani, J.F., Samborska, B., Lu, G.Z., Jedrychowski, M.P., Lajoie, M., Zhang, S., Ramsay, L.C., Dou, F.Y., Tenen, D., et al. (2019). Ablation of adipocyte creatine transport impairs thermogenesis and causes diet-induced obesity. Nat. Metab. *1*, 360–370.

Kim, J., Cho, Y.J., Ryu, J.Y., Hwang, I., Han, H.D., Ahn, H.J., Kim, W.Y., Cho, H., Chung, J.Y., Hewitt, S.M., et al. (2020). CDK7 is a reliable prognostic factor and novel therapeutic target in epithelial ovarian cancer. Gynecol. Oncol. *156*, 211–221.

Kir, S., White, J.P., Kleiner, S., Kazak, L., Cohen, P., Baracos, V.E., and Spiegelman, B.M. (2014). Tumour-derived PTH-related protein triggers adipose tissue browning and cancer cachexia. Nature *513*, 100–104.

Kwiatkowski, N., Zhang, T., Rahl, P.B., Abraham, B.J., Reddy, J., Ficarro, S.B., Dastur, A., Amzallag, A., Ramaswamy, S., Tesar, B., et al. (2014). Targeting transcription regulation in cancer with a covalent CDK7 inhibitor. Nature *511*, 616–620.

Lagarrigue, S., Lopez-Mejia, I.C., Denechaud, P.D., Escote, X., Castillo-Armengol, J., Jimenez, V., Chavey, C., Giralt, A., Lai, Q., Zhang, L., et al. (2016). CDK4 is an essential insulin effector in adipocytes. J. Clin. Invest. *126*, 335–348.

Liu, X., Rossmeisl, M., McClaine, J., Riachi, M., Harper, M.E., and Kozak, L.P. (2003). Paradoxical resistance to diet-induced obesity in UCP1-deficient mice. J. Clin. Invest. *111*, 399–407.

Lopez-Mejia, I.C., Castillo-Armengol, J., Lagarrigue, S., and Fajas, L. (2018). Role of cell cycle regulators in adipose tissue and whole body energy homeostasis. Cell. Mol. Life Sci. *75*, 975–987.

Lopez-Mejia, I.C., Lagarrigue, S., Giralt, A., Martinez-Carreres, L., Zanou, N., Denechaud, P.D., Castillo-Armengol, J., Chavey, C., Orpinell, M., Delacuisine, B., et al. (2017). CDK4 phosphorylates AMPKalpha2 to inhibit its activity and repress fatty acid oxidation. Mol. Cell *68*, 336–349 e6.

Makela, T.P., Tassan, J.P., Nigg, E.A., Frutiger, S., Hughes, G.J., and Weinberg, R.A. (1994). A cyclin associated with the CDK-activating kinase MO15. Nature *371*, 254–257.

Malumbres, M., and Barbacid, M. (2005). Mammalian cyclin-dependent kinases. Trends Biochem. Sci. *30*, 630–641.

Mottillo, E.P., Shen, X.J., and Granneman, J.G. (2010). beta3-adrenergic receptor induction of adipocyte inflammation requires lipolytic activation of stress kinases p38 and JNK. Biochim. Biophys. Acta *1801*, 1048–1055.

Murray, A.W. (2004). Recycling the cell cycle: cyclins revisited. Cell *116*, 221–234.

Nilson, K.A., Guo, J., Turek, M.E., Brogie, J.E., Delaney, E., Luse, D.S., and Price, D.H. (2015). THZ1 reveals roles for Cdk7 in Co-transcriptional capping and pausing. Mol. Cell *59*, 576–587.

Rasool, R.U., Natesan, R., Deng, Q., Aras, S., Lal, P., Sander Effron, S., Mitchell-Velasquez, E., Posimo, J.M., Carskadon, S., Baca, S.C., et al. (2019). CDK7 inhibition suppresses castration-resistant prostate cancer through MED1 inactivation. Cancer Discov. *9*, 1538–1555.

Sanchez-Gurmaches, J., Tang, Y., Jespersen, N.Z., Wallace, M., Martinez Calejman, C., Gujja, S., Li, H., Edwards, Y.J.K., Wolfrum, C., Metallo, C.M., et al. (2018). Brown fat AKT2 is a cold-induced kinase that stimulates ChREBP-mediated de novo lipogenesis to optimize fuel storage and thermogenesis. Cell Metab. *27*, 195–209.e6.

Sano, M., Izumi, Y., Helenius, K., Asakura, M., Rossi, D.J., Xie, M., Taffet, G., Hu, L., Pautler, R.G., Wilson, C.R., et al. (2007). Menage-a-trois 1 is critical for the transcriptional function of PPARgamma coactivator 1. Cell Metab. *5*, 129–142.

Schreiber, R., Diwoky, C., Schoiswohl, G., Feiler, U., Wongsiriroj, N., Abdellatif, M., Kolb, D., Hoeks, J., Kershaw, E.E., Sedej, S., et al. (2017). Cold-induced thermogenesis depends on ATGL-mediated lipolysis in cardiac muscle, but not Brown adipose tissue. Cell Metab. *26*, 753–763.e7.

Shellock, F.G., Riedinger, M.S., and Fishbein, M.C. (1986). Brown adipose tissue in cancer patients: possible cause of cancer-induced cachexia. J. Cancer Res. Clin. Oncol. *111*, 82–85.

Shiekhattar, R., Mermelstein, F., Fisher, R.P., Drapkin, R., Dynlacht, B., Wessling, H.C., Morgan, D.O., and Reinberg, D. (1995). Cdk-activating kinase complex is a component of human transcription factor TFIIH. Nature *374*, 283–287.

Shin, H., Ma, Y., Chanturiya, T., Cao, Q., Wang, Y., Kadegowda, A.K.G., Jackson, R., Rumore, D., Xue, B., Shi, H., et al. (2017). Lipolysis in Brown adipocytes is not essential for cold-induced thermogenesis in mice. Cell Metab. *26*, 764–777.e5.

Sun, B., Mason, S., Wilson, R.C., Hazard, S.E., Wang, Y., Fang, R., Wang, Q., Yeh, E.S., Yang, M., Roberts, T.M., et al. (2020). Inhibition of the transcriptional kinase CDK7 overcomes therapeutic resistance in HER2-positive breast cancers. Oncogene *39*, 50–63.

Yee, A., Nichols, M.A., Wu, L., Hall, F.L., Kobayashi, R., and Xiong, Y. (1995). Molecular cloning of CDK7-associated human MAT1, a cyclin-dependent kinase-activating kinase (CAK) assembly factor. Cancer Res. *55*, 6058–6062.

Yu, X.X., Lewin, D.A., Forrest, W., and Adams, S.H. (2002). Cold elicits the simultaneous induction of fatty acid synthesis and beta-oxidation in murine brown adipose tissue: prediction from differential gene expression and confirmation in vivo. FASEB J. *16*, 155–168.

Zhang, H., Christensen, C.L., Dries, R., Oser, M.G., Deng, J., Diskin, B., Li, F., Pan, Y., Zhang, X., Yin, Y., et al. (2020). CDK7 inhibition potentiates genome instability triggering anti-tumor immunity in small cell lung cancer. Cancer Cell *37*, 37–54.e9.

iScience, Volume *23*

Supplemental Information

CDK7 Mediates the Beta-Adrenergic Signaling in Thermogenic Brown and White Adipose Tissues

Honglei Ji, Yizhe Chen, Judit Castillo-Armengol, René Dreos, Catherine Moret, Guy Niederhäuser, Brigitte Delacuisine, Isabel C. Lopez-Mejia, Pierre-Damien Denechaud, and Lluis Fajas

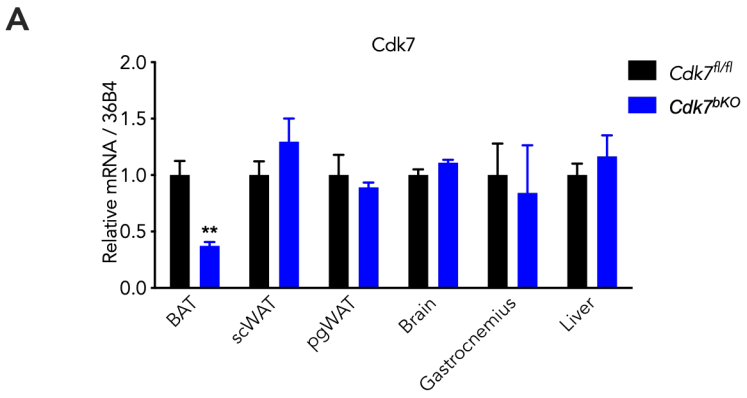

Figure S1. Generation of CDK7 brown fat specific knockout mice model. Related to Figure 1. (A) qPCR analysis of *Cdk7* expression in various tissues in *Cdk7*^{bKO} and control littermates in fed state (male, n=3, 9-11w). All values represent means ± SEM. **p<0.01.

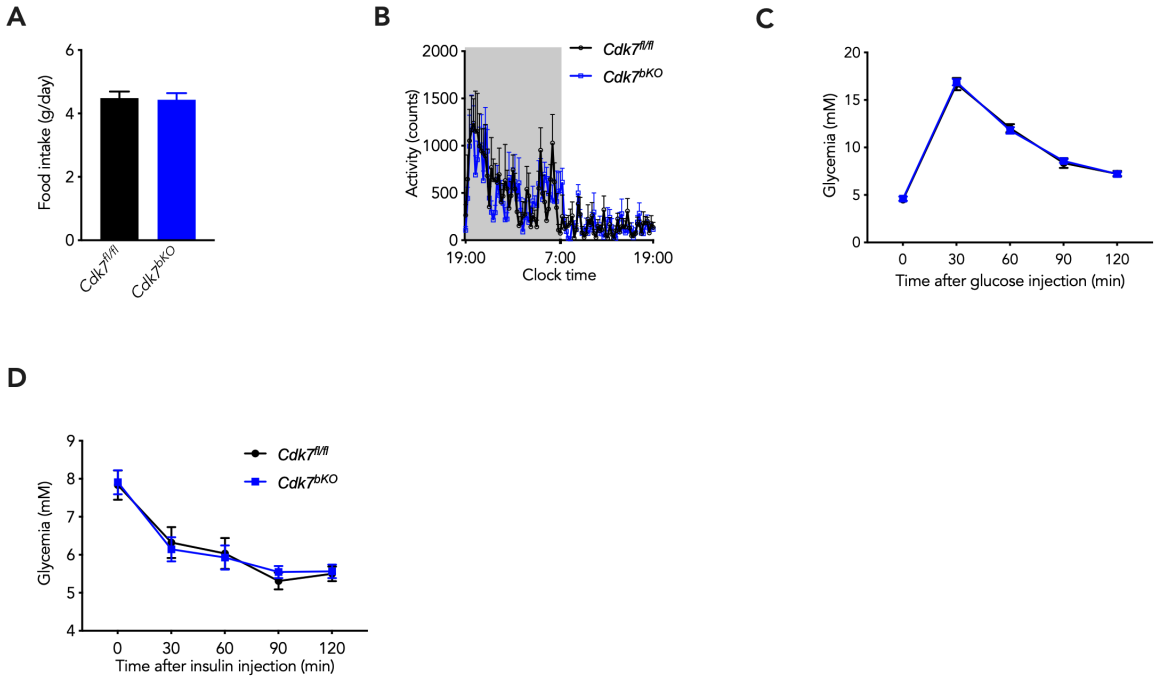

Figure S2. Energy homeostasis in *Cdk7^{bKO}* mice. Related to Figure 1. Food intake (A), physical activity (B) were measured during indirect calorimetry tests using a comprehensive laboratory animal monitoring system (CLAMS). (male, 8w, n = 6 for each group). Glucose tolerance test (C) and insulin tolerance test (D) in wild-type and *Cdk7^{bKO}* mice (male, 10w, n = 9-11 for each group).

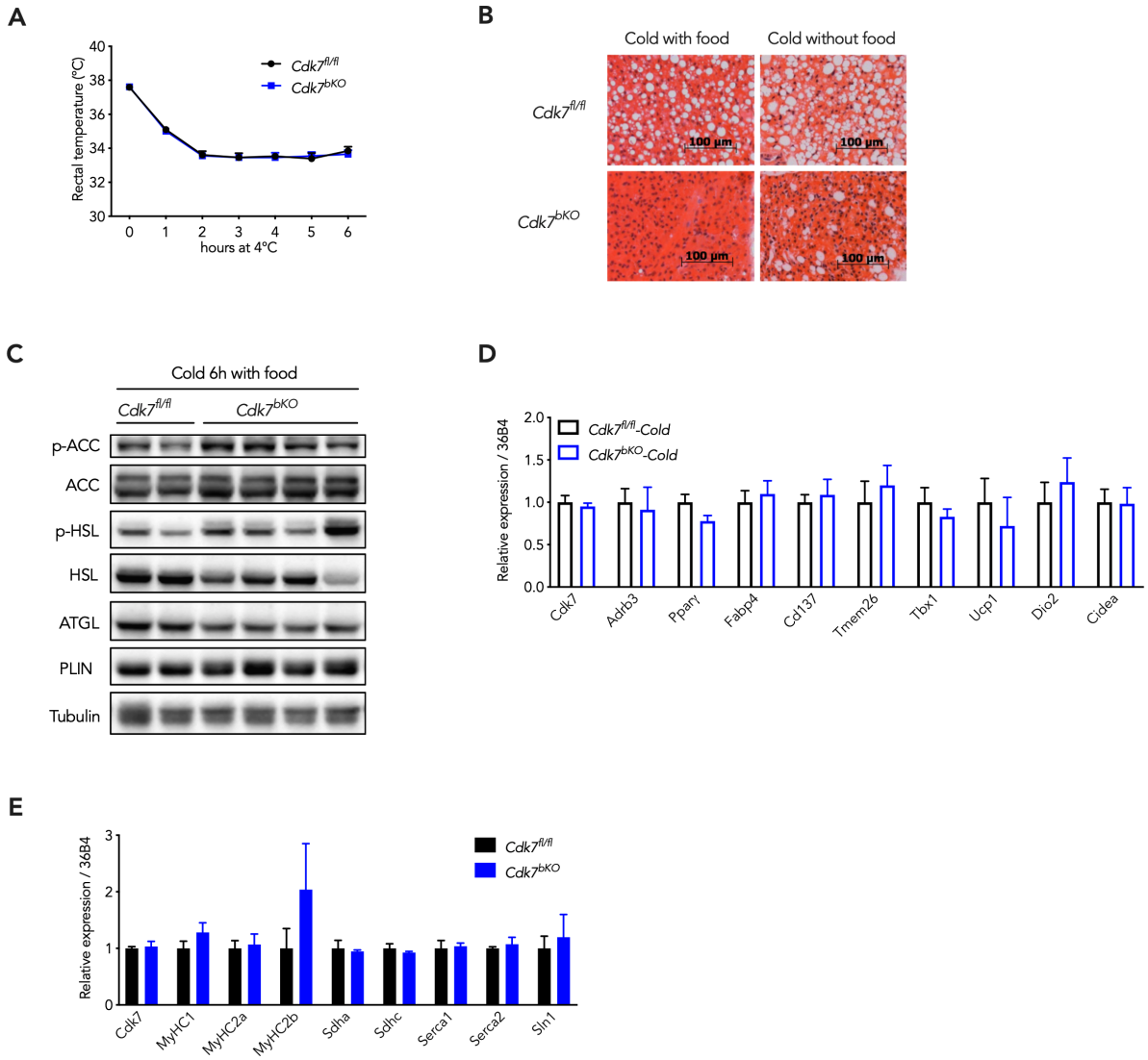

Figure S3. BAT dysfunction in *Cdk7*^{bKO} mice does not leads to compensatory browning of white fat or alteration of muscle metabolism. Related to Figure 2 and 3. (A) Acute cold response of *Cdk7*^{bKO} and *Cdk7*$^{fl/fl}$ mice was performed with food supply to evaluate thermogenic activity (male, 6-8w, n = 8 for each group). (B) H&E staining of BAT in response to cold with or without food (scale bar, 100 μm). (C) Lipolysis related protein markers in BAT of *Cdk7*^{bKO} and *Cdk7*$^{fl/fl}$ in response to a cold test with food. (D) Browning related marker genes in scWAT after 6 hours of cold exposure were analyzed by qPCR (male, 20w, n = 7-8 for each group). (E) Muscle metabolism related marker genes were analyzed by qPCR in soleus muscle at room temperature (male, 13w, n = 3 for each group).

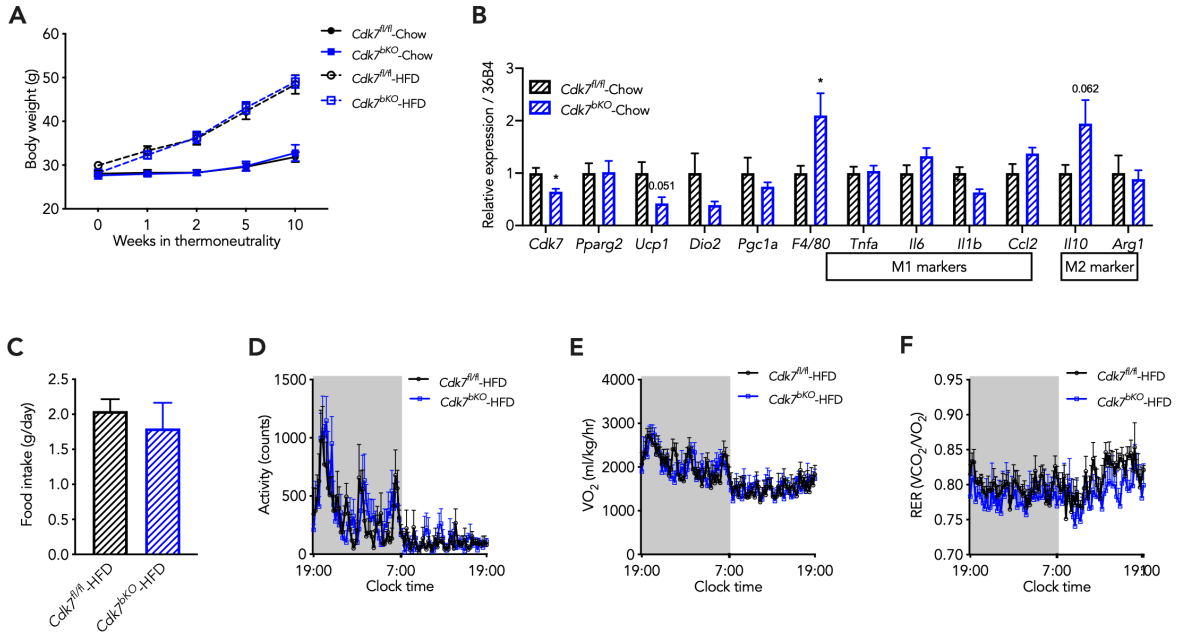

Figure S4. Effect of thermoneutrality on *Cdk7^{bKO}* mouse models. Related to Figure 4. 12-14 weeks old weight-matched *Cdk7^{bKO}* and control littermates were put in thermoneutrality (30°C) on chow or HFD for 10 weeks. (A) Weight gain was recorded (n = 6-8 for each group). (B) mRNA expression of genes in BAT of *Cdk7^{bKO}* and *Cdk7$^{fl/fl}$* mice after 10 weeks at thermoneutrality on chow diet. Food intake (C), physical activity (D), oxygen consumption (E) were measured during indirect calorimetry with mice after three weeks at thermoneutrality on HFD. The respiratory exchange ratio (RER) (F) is calculated as the ratio between VCO_2 and VO_2 (male, 8w, n = 6 for each group).

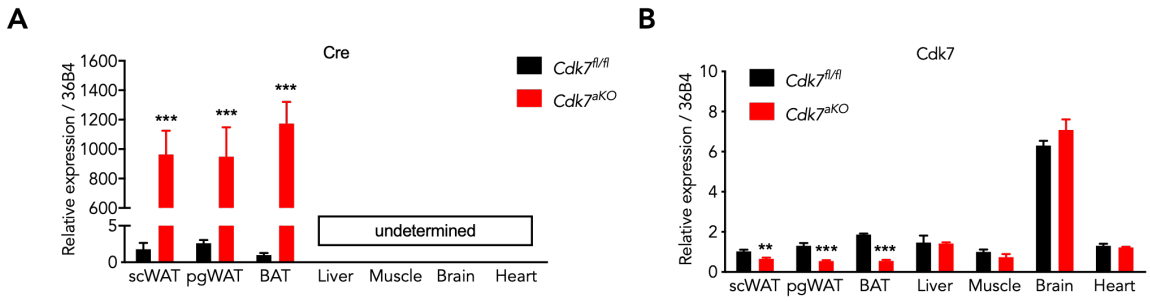

Figure S5. Generation of CDK7 adipocytes specific knock out mice model. Related to Figure 5. (A) *Cre* and *Cdk7* (B) expression in various tissues of $Cdk7^{fl/fl}$ and $Cdk7^{aKO}$ mice analysed by qPCR (male, 14 weeks old, n = 5-7). Values represent means ± SEM. **p<0.01, ***p<0.001.

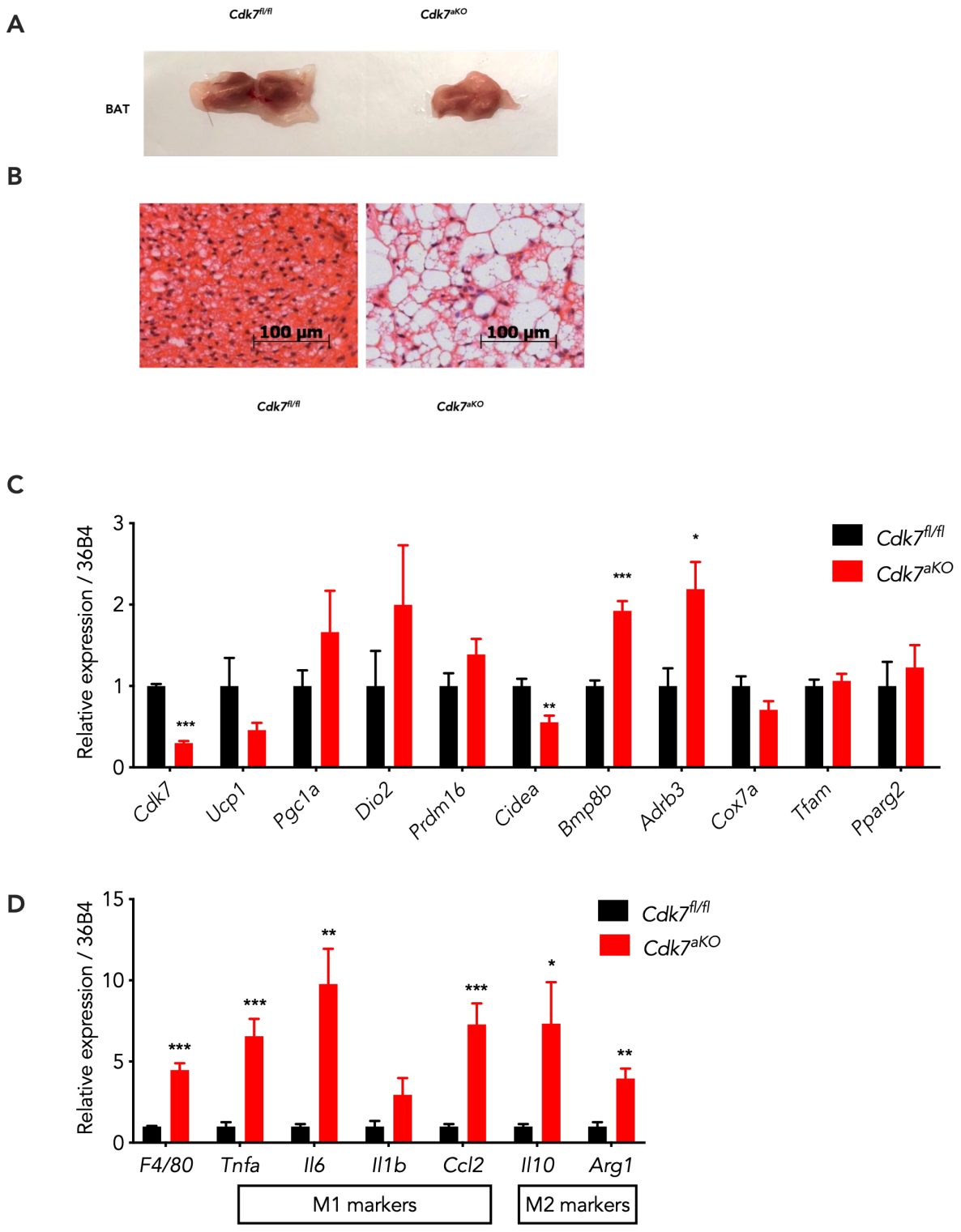

Figure S6. BAT phenotypes in Cdk7aKO mice. Related to Figure 5. (A) Brown adipose tissue (BAT) pictures from male control *Cdk7*$^{fl/fl}$ and *Cdk7*^{aKO} mice at room temperature (male, 14w). (B) Hematoxylin/eosin staining of BAT. (C) Quantitative PCR analysis of the expression of *Ucp1* and other BAT marker genes at room temperature (male, 14w, n = 7 for each group). (D) M1 and M2 macrophages markers were analyzed by qPCR (male, 14w, n = 7 for each group). Values represent means ± SEM. *p<0.05, **p<0.01, ***p<0.001.

Table S1. Selected genes expression from the intersection data in Fig. 6C. Related to Figure 6.

Up-regulated genes

	AdipoQ cre				UCP1 cre			
Name	Average Expression	log2 Fold Change	Standard Error	p-adj	Average Expression	log2 Fold Change	Standard Error	p-adj
Il15	373.5253231	0.830143334	0.191756917	1.42E-05	122.7029248	1.167399941	0.396085873	0.000123911
Cdk6	579.2126462	1.127359833	0.235355135	7.00E-07	286.5481096	0.738993865	0.205438204	0.000207604
Cdk19	906.6483902	0.69644509	0.161481011	1.94E-05	424.7865619	0.956101576	0.165434389	4.30E-09
Lrp1	19798.38816	2.165744872	0.186544941	6.74E-31	3375.698697	0.780775649	0.15385524	6.30E-07

Down-regulated genes

	AdipoQ cre				UCP1 cre			
Name	Average Expression	log2 Fold Change	Standard Error	p-adj	Average Expression	log2 Fold Change	Standard Error	p-adj
Dio2	139.8557436	-0.916078047	0.447610711	0.009701702	50947.72267	-0.724935087	0.487790255	0.013402778
Plin5	212.3179108	-1.070529291	0.30351079	0.000122504	4658.017282	-0.629845195	0.134940403	1.10E-05
Lpin1	13018.93145	-1.08098165	0.185356344	4.48E-09	14602.24324	-0.84292194	0.132482306	4.84E-10
Lipg	250.2707685	-1.552928099	0.712566083	0.001662095	974.1311456	-1.149929633	0.462593712	0.000414196
Gk	954.690291	-1.164155378	0.300349323	2.50E-05	26023.6271	-0.521081848	0.205740534	0.012724041
Gpam	8284.208457	-0.694709582	0.2117277	0.000819294	15710.10642	-1.010738464	0.160996295	1.78E-10
Gpat4	5018.744126	-0.564037596	0.139255619	6.71E-05	17010.10433	-0.654921599	0.17676147	0.000277591
Ppargc1a	314.5589381	-1.114646546	0.26677138	9.75E-06	18338.22693	-1.956655202	0.615646463	1.14E-05
Adrb1	36.36978979	-1.347026273	0.503851018	0.000638917	797.817873	-0.742497057	0.221798319	0.000427506
Adrb3	10959.08836	-1.957675013	0.139274755	8.77E-45	2908.040196	-1.280950536	0.572232655	0.000435321
Dgat1	8667.841719	-1.201865856	0.161195529	7.18E-14	17166.85086	-0.923479619	0.190848378	5.26E-07
Adcy4	650.272503	-0.557507713	0.169778815	0.001047374	1218.543836	-0.855346505	0.163846453	1.64E-07

Table S2. Primer list in qPCR. Related to Figure 3-5 and Figure S1, S3-6.

Gene	Primer sequence
36B4 (Rplp0)	F: 5'-AGATTCGGGATATGCTGTTGG-3' R: 5'-AAAGCCTGGAAGAAGGAGGTC-3'
Adrb3	F: 5'-CACCGCTCAACAGGTTTGATG-3' R: 5'-TCTTGGGGCAACCAGTCAAG-3'
Arg1	F: 5'-CTCCAAGCCAAAGTCCTTAGAG-3' R: 5'-AGGAGCTGTCATTAGGGACATC-3'
Atp5g	F: 5'-GAGTCAGTCACCTTGAGCAGG-3' R: 5'-CTGGTACAGGAGCGAATCAGA-3'
Bmp8b	F: 5'-CTCTTCCAAGGCAGGAAAC-3' R: 5'-GAGATGAGAGATGGGCTACT-3'
CD137 (Tnfrsf9)	F: 5'-TGGGTCAGGGGTTCTGAGTTC-3' R: 5'-CTTCTCACAGCCCACTAGCAG-3'
Cdk7	F: 5'-CAGTTTGCGACGGTCTATAA-3' R: 5'-CTCCCTTAAGGCTGTTCTATTT-3'
Cidea	F: 5'-TGCTCTTCTGTATCGCCCAGT-3' R: 5'-GCCGTGTTAAGGAATCTGCTG-3'
Ckmt1	F: 5'-CATGTGGAATGAGCGTTTAGG-3' R: 5'- TTTGGGAAGCGGTTATCTTTG -3'
Ckmt2	F: 5'-TGAGGAGTCGTATGAGGTATTT-3' R: 5'-AACTGCCCGTGAGTAATCT-3'
Cre	F: 5'-ACGTTCACCGGCATCAACGT-3' R: 5'-CACGACCAAGTGACAGCAATG-3'
Dio2	F: 5'-CAAACAGGTTAAACTGGGTGAAGA-3' R: 5'-GTCAAGAAGGTGGCATTCGG-3'
F4/80 (Adgre1)	F: 5'-AAGACTTGATACTCCAAAGTGAGC-3' R: 5'-GAAGGAAGCATAACCAAGATCCC-3'
Fabp4	F: 5'-AACACCGAGATTTCCTTCAA-3' R: 5'-AGTCACGCCTTTCATAACACA-3'
Gamt	F: 5'-CCCATAGAGGAACACTGGATTAT-3' R: 5'-CCTTTCAAGGGAACAACCTTATG-3'
Gatm	F: 5'-CTTTGAGTACCGAGCGTACAG-3' R: 5'-GGATGGGATAATTCTGGTCATACA-3'
Il1b	F: 5'-GCAACTGTTCCTGAACTCAACT-3' R: 5'-ATCTTTTGGGGTCCGTCAACT-3'
Il6	F: 5'-CTTCCATCCAGTTGCCTTCT -3' R: 5'-CTCCGACTTGTGAAGTGGTATAG-3'
Il10	F: 5'-GCTCTTACTGACTGGCATGAG-3' R: 5'-CGCAGCTCTAGGAGCATGTG-3'
Ccl2	F: 5'-CCACTCACCTGCTGCTACTCA-3' R: 5'-TGGTGATCCTCTTGTAGCTCTCC-3'
MyHC1	F: 5'-CCAAGGGCCTGAATGAGGAG-3' R: 5'-GCAAAGGCTCCAGGTCTGAG-3'
MyHC2a	F: 5'-AAGCGAAGAGTAAGGCTGTC-3' R: 5'-GTGATTGCTTGCAAAGGAAC-3'

MyHC2b	F: 5’-ACAAGCTGCGGGTGAAGAGC-3' R: 5’-CAGGACAGTGACAAAGAACG-3'
Pgc1a	F: 5’-CCGATCACCATATTCCAGGTC-3’ R: 5’-GTGTGCGGTGTCTGTAGTGG-3’
Phospho1	F: 5’-GCTGGAGACCAACAGTTTCTAA-3' R: 5’-CATCCTGCCGTCCCTAGATA -3'
Pparg2	F: 5’-CACCAGTGTGAATTACAGCAAATC-3’ R: 5’-AGCTGATTCCGAAGTTGGTG-3’
Prdm16	F: 5’-CAGCACGGTGAAGCCATTC-3’ R: 5’-GCGTGCATCCGCTTGTG-3’
Sdha	F: 5’-GAAAGGCGGGCAGGCTCATC-3' R: 5’-CACCACGGCACTCCCCATTTT-3'
Serca1(Atp2a1)	F: 5’-GACCTGCTTGTGCGGATTCTT-3' R: 5’-CAATGGCGTTGGCAATGAGC-3'
Serca2(Atp2a2)	F: 5’-ATGGAGAACGCTCACACAAAG-3' R: 5’-ACTGCTCAATCACAAGTTCCAG-3'
Slc6a8	F: 5’-CGAGTTCTGGGAGAACAAAGT-3' R: 5’-CCTTCCACACACAGAAGTAGAC-3'
Sln	F: 5’-CAGACATTCTGAAGATGGAGAG-3' R: 5’-CATAAGGAGAACGGTGATGAG-3'
Tbx1	F: 5’-AGATGATCGTCACCAAGGCAG-3' R: 5’-TCATCTACGGGCACAAAGTCC-3'
Tmem26	F: 5’-TCTGATGTTTGTGGGGACGG-3' R: 5’-CAAGGGGGAACTGCAGCATA-3'
Tnf	F: 5’-CGTGGAACTGGCAGAAGAG-3' R: 5’-ACAAGCAGGAATGAGAAGAGG-3'
Ucp1	F: 5’-CACCTTCCCGCTGGACACTGC-3’ R: 5’-TTGCCAGGGTGGTGATGGTCC-3’

Transparent methods

Animals. *Cdk7* floxed mice (*Cdk7*$^{fl/+}$) were gifts from D. Santamaria and M. Barbacid at the CNIO (Madrid, Spain). *Cdk7*$^{fl/fl}$ mice were crossed to the Ucp1-Cre (JAX no.024670) or Adipoq-Cre (JAX no.010803) transgenic strains to obtain Cre positive *Cdk7*$^{fl/+}$, and after another backcross to obtain *Cdk7*$^{fl/fl}$ Ucp1-Cre positive (refered to as *Cdk7*^{bKO}) and littermates *Cdk7*$^{fl/fl}$ Ucp1-Cre negative control mice or *Cdk7*$^{fl/fl}$ Adipoq-Cre positive (refered to as *Cdk7*^{aKO}) and littermates *Cdk7*$^{fl/fl}$ Adipoq-Cre negative control mice. Mice were maintained in a temperature-controlled animal facility with a 12-hour light/12-hour dark cycle and had access to standard chow (KLIBA NAFAG no.3436) and water according to Swiss Animal Protection Ordinance (OPAn). High-fat diet studies were conducted by feeding mice a purified-ingredient diet (ENVIGO, TD.06414) at 6 weeks old for 16 weeks.

Body composition. Body composition was determined with EchoMRI.

Glucose tolerance test (GTT) and insulin tolerance test (ITT). For GTT, mice were starved for 16 hours and then administered intraperitoneal (i.p.) injection with glucose (2g/kg body weight). Tail vein blood glucose level was measured at the indicated times. For ITT, 6-hour fasted mice were injected i.p. with insulin (0.75U/kg body weight), and tail vein blood glucose levels were then measured at the indicated times. Actrapid® human recombinant insulin was purchased from Novo Nordisk Pharma SA.

Indirect calorimetry. Oxygen consumption (VO_2), carbon dioxide production (VCO_2), food intake and activity were monitored by indirect calorimetry using the Comprehensive Laboratory Animal Monitoring System (CLAMS; Columbus Instruments, Columbus, OH, USA). Energy expenditure (EE) was estimated using VO_2 and VCO_2 values from indirect calorimetry, using the following equation EE (in kcal/h) = $(3.815 \times VO_2) + (1.232 \times VCO_2)$.

Cold-tolerance test. Baseline measurements of internal core body temperatures were recorded from ad libitum fed mice at room temperature (22 °C) (starting at zeitgeber time 3) using a digital thermometer (Bioseb) coupled with a probe. Mice were then housed in individual cages with water and minimum bedding and transferred to 4 °C cold room. Food was presence or removed depending on the experimental setup. Rectal temperature and glycemia were measured at indicated time points. Individual mice were removed from the study if core body temperature fell below 30 °C.

Thermoneutrality adaptation. For acclimation to thermoneutrality, mice were transferred to a room with controlled ambient temperature at 30 °C and a humidity of 40-60% for 10 weeks. Mice were single-housed and had free access to food and water unless otherwise stated.

CL-316,243 treatment. CL-316,243 (Abcam, ab144605), a selective β3-adrenoceptor agonist was used to maximally stimulate facultative thermogenesis during indirect calorimetry, or induce white adipose tissue browning after long-term treatment. The acute stimulation on CDK7 flox/flox Ucp1-Cre mice were performed at thermoneutrality (30 °C) to eliminate endogenous BAT activation. To minimize the stress initiated by injection, the animals were anesthetized with pentobarbital (90 mg/kg, i.p.), and indirect calorimetry was performed with CLAMS (Columbus Instruments, Columbus, OH) for 40-50 min at 30 °C to obtain basal values (Golozoubova, Cannon, and Nedergaard 2006). Then mice were injected with CL-316,243 (1mg/kg in saline, i.p.), and immediately returned to the chamber, and oxygen consumption was measured for another 40-50 min. For the long-term treatment on CDK7 flox/flox Adiponectin-Cre mice, which were injected CL-316,243 (1 mg/kg body weight, i.p.) or an equivalent volume of sterile saline for 7 days, and sacrificed on day eight.

Mice sacrifice. The mice were sacrificed at indicated time with cervical dislocation and blood was collected by cardiac puncture, and tissues were harvested, weighed, and flash-frozen in liquid nitrogen or fixed with 4% formalin to perform biochemical and histologic analyses, respectively. For all studies, age- and sex-matched littermates were used as controls. The specific age and number of the mice for each experiment were indicated in the figure legend. All the mouse experiments were authorized by the Veterinary Office of the Canton of Vaud, Switzerland under the license no. VD2627 and VD3121.

Blood analysis. Blood glucose concentrations were measured with glucose test strips (Roche). Plasma NEFA levels were measured by WAKO NEFA KIT. Plasma glycerol levels were determined by Free Glycerol Determination KIT from Sigma.

Histology. The hematoxylin **and** eosin staining was performed in formalin-fixed paraffin-embedded tissue sections. Primary antibodies anti-UCP1 (ab10983, Abcam) and anti-F4/80 (ab6640, Abcam) were used for immunohistochemical analysis. For immunostaining and colorations, the adipose tissue was sectioned into 4-µm-thick paraffin sections. For immunostaining, sections were incubated overnight with the respective primary antibodies.

RNA extraction and RT-qPCR. For gene expression analysis, RNA was isolated with TRI Reagent (Sigma-Aldrich, T9424) according to the manufacturer's protocol. RNA (1 µg) was

subsequently reverse-transcribed with SuperScript™ II Reverse Transcriptase (Thermo Fisher Scientific, 18064014). qPCR was performed using ABI 7900 HT and SYBER Green Master Mix (Roche, 04913914001) for detection. Fold change was determined by comparing target gene expression with the reference genes RS9 or 36B4. Relative mRNA fold changes between groups were calculated via the ΔCt method. The sequences of primers that were used for qPCR are in supplemental table S2.

Protein extraction and western blotting. Protein extracts were isolated with M-PER (Thermo Fisher, 78501) and quantified with BCA Protein Assay Kit (Thermo Fisher, 23225). For Western blotting, proteins were separated by SDS-PAGE and transferred onto nitrocellulose membranes. The following antibodies were used: CDK7 (SANTA CRUZ, sc-7344); UCP1 (Abcam, ab10983); PGC1 α (Abcam, ab54481); p-ACC (Ser79) (Merck, 07-303); ACC (CST, 3662S); p-HSL (Ser563) (CST, 4139S); HSL (SANTA CRUZ, sc-25843); ATGL (CST, 2138S); Perilipin A (Abcam, ab61682); Tubulin (Sigma, T6199).

RNA-seq library preparation. Interscapular BAT pads were taken from 12-week-old *Cdk7*^{bKO} and control littermates either at room temperature or after 6 hours of cold exposure with food. Mice were sacrificed at zeitgeber time 9. Total RNA was extracted with TRI Reagent (Sigma-Aldrich, T9424). Two RNA samples from two mice with same genotype and condition were pool together (each 250 ng) to constitute 500 ng of total RNA from biological triplicates (three *Cdk7*$^{fl/fl}$-RT, three *Cdk7*^{bKO}-RT, three *Cdk7*$^{fl/fl}$-cold, and three *Cdk7*^{bKO}-cold) for sequencing. Perigonadal WAT of *Cdk7*^{aKO} mice were taken after 7 days CL-316,243 treatment. The RNA extraction method was the same as mentioned above. Similarly, two RNA samples from two mice with same genotype and treatment were pooled together (each 250 ng) to constitute 500 ng of total RNA from biological triplicates (three *Cdk7*$^{fl/fl}$-saline, three *Cdk7*^{aKO}-saline, three *Cdk7*$^{fl/fl}$-CL, and three *Cdk7*^{aKO}-CL) for sequencing.

RNA-seq data analysis. Purity-filtered reads were adapters and quality trimmed with Cutadapt (v. 1.8, Martin 2011). Reads matching to ribosomal RNA sequences were removed with fastq_screen (v. 0.9.3). Remaining read were further filtered for low complexity with reapers (v. 15-065, (Davis et al. 2013)). Reads were aligned against Mus musculus. GRCm38.86 genome using STAR (v. 2.5.2b, (Dobin et al. 2013)). The number of red counts per gene locus was summarized with htseq-count (v. 0.6.1, (Anders, Pyl, and Huber 2015)) using Mus musculus. GRCm38.86 gene annotation. Quality of the RNA-seq data alignment was assessed using RSeQC (v. 2.3.7, (Wang, Wang, and Li 2012)). Reads were also aligned to the Mus musculus.GRCm38.86 transcriptome using STAR (v. 2.5.2b, (Dobin et al. 2013)) and the

estimation of the isoforms abundance was computed using RSEM (v. 1.2.31, (Li and Dewey 2011)). Genes were included in differential expression analysis if their expression levels were>1 RPKM in at least one sample. Genes having a FDR of <0.05 were selected as significantly regulated genes. Representative down-regulated genes identified by Gene Ontology were presented with their log2 (fold change) as a heat map. The pathway analysis in Fig. 3D, E and 6D was using the R package ReactomePA (Yu and He 2016) with default parameters.

GPA injection. On the first day, 8-week-old male *Cdk7*^{bKO} and littermate control mice (*Cdk7*$^{fl/fl}$) were separated one per cage. Basal rectal temperature was measured at zeitgeber time 8. On the second day, the isolated mice were transferred to a cold chamber at ambient temperature 18 °C for one-day cold acclimation. Basal rectal temperature was measured at zeitgeber time 8. At the beginning of the third day, the chamber temperature was switched to 4 °C and maintained for four days. During the four days at zeitgeber time 6, mice were given daily injections with a dose of β-GPA (0.4 g/kg, i.p.) or saline control. Two hours after injection at zeitgeber time 8, rectal temperature was monitored. On the last day at zeitgeber time 9, mice were sacrificed by cervical dislocation, blood and adipose tissues were collected. Body weight and glycemia were also measured at the first day and last day of the experiment at zeitgeber time 8.

Statistical analysis. Data were presented as mean ± SEM. Statistical analyses were performed with Prism software (GraphPad). Differences between two groups were analyzed using Student's t-test (two-tailed), and multiple comparisons were analyzed by ANOVA with a Tukey post hoc test. Statistical parameters (i.e. p values, numbers of biological repeats) can be found in the figure legends. Differences were considered statistically significant at $p < 0.05$.

Supplemental references

Anders, S., P. T. Pyl, and W. Huber. 2015. 'HTSeq--a Python framework to work with high-throughput sequencing data', *Bioinformatics*, 31: 166-9.

Davis, M. P., S. van Dongen, C. Abreu-Goodger, N. Bartonicek, and A. J. Enright. 2013. 'Kraken: a set of tools for quality control and analysis of high-throughput sequence data', *Methods*, 63: 41-9.

Dobin, A., C. A. Davis, F. Schlesinger, J. Drenkow, C. Zaleski, S. Jha, P. Batut, M. Chaisson, and T. R. Gingeras. 2013. 'STAR: ultrafast universal RNA-seq aligner', *Bioinformatics*, 29: 15-21.

Golozoubova, V., B. Cannon, and J. Nedergaard. 2006. 'UCP1 is essential for adaptive adrenergic nonshivering thermogenesis', *Am J Physiol Endocrinol Metab*, 291: E350-7.
Li, B., and C. N. Dewey. 2011. 'RSEM: accurate transcript quantification from RNA-Seq data with or without a reference genome', *BMC Bioinformatics*, 12: 323.
Wang, L., S. Wang, and W. Li. 2012. 'RSeQC: quality control of RNA-seq experiments', *Bioinformatics*, 28: 2184-5.
Yu, G., and Q. Y. He. 2016. 'ReactomePA: an R/Bioconductor package for reactome pathway analysis and visualization', *Mol Biosyst*, 12: 477-9.